Microporous and Mesoporous Materials 258 (2018) 151–169

Contents lists available at ScienceDirect

Microporous and Mesoporous Materials

journal homepage: www.elsevier.com/locate/micromeso

Using Molecular Dynamics simulations for elucidation of molecular traffic in ordered crystalline microporous materials

Rajamani Krishna [a, *], Jasper M. van Baten [b]

[a] Van 't Hoff Institute for Molecular Sciences, University of Amsterdam, Science Park 904, 1098 XH Amsterdam, The Netherlands
[b] AmsterCHEM, Calle Las Rozas 32, 04618 Las Rozas, Cuevas del Almanzora, Almería, Spain

ARTICLE INFO

Article history:
Received 30 July 2017
Received in revised form
23 August 2017
Accepted 13 September 2017
Available online 18 September 2017

Keywords:
Molecular traffic
Mixture diffusion
Zeolites
Traffic junction effects
Hindering effects
Inter-cage hopping
Correlations between molecular jumps
Mutual slowing-down

ABSTRACT

Robust models to describe mixture diffusion in ordered crystalline microporous materials such as zeolites, metal-organic frameworks (MOFs), and zeolitic imidazolate frameworks (ZIFs) are essential for the development of separation and reaction technologies. The development of appropriate models requires insights into a wide variety of factors that influence the mobilities of guest molecules in the microporous hosts. Such factors include: molecular size, shape, and configuration, degree of confinement, pore topology and connectivity, strength of adsorption on pore walls, molar loadings of guest constituents, and correlations in the molecular jumps between partner molecules. Experimental data, on their own, do not provide sufficient information to set up the requisite models to describe mixture diffusion. The primary objective of this article is to demonstrate the potency of Molecular Dynamics (MD) simulations to offer insights that assist in the interpretation of experimental observations and development of descriptive models. Computational snapshots and video animations are used to provide a visual appreciation of phenomena such as traffic junction, slowing-down, and hindering effects in diffusion.

1. Introduction

Ordered crystalline microporous materials such as zeolites (crystalline alumino-silicates), metal-organic frameworks (MOFs), covalent organic frameworks (COFs), and zeolitic imidazolate frameworks (ZIFs) offer the potential for use as adsorbents or catalysts in several separation and reaction technologies, that are of interest in the process industries [1–10]. Such materials can also be employed as thin layers, with thickness of the order of the order of a few tens of micrometers, in membrane devices [11,12].

For reaction and separation process design and development, it is necessary to have reliable models to describe diffusion of mixtures of guest molecules inside the microporous materials. The proper description of diffusion is important for the following reasons.

- In many membrane separations, the permeation selectivity is significantly influenced by the relative mobilities of the adsorbed species within the pores. Indeed, in H_2-selective membrane processes, the separation relies on the fact that H_2 is more mobile than partner species such as CO_2, or CH_4 [13–15].
- The separation performance of microporous adsorbents in fixed bed devices may be influenced by intra-crystalline diffusion limitations; such diffusion influences result in transient breakthroughs that possess distended characteristics and diminished separation capabilities [3,16,17].
- In some cases of pressure swing adsorption, the separation principle is based on diffusion selectivities; this is the case for example for separation of N_2/O_2 mixtures with LTA-4A zeolite [3,17].
- In catalytic processes, intra-crystalline diffusional effects affect both reaction rates and selectivities. Often, diffusional effects are undesirable because catalyst effectiveness is reduced [5,18,19].

A number of different channel topologies and connectivities are encountered in zeolites, MOFs, COFs, and ZIFs. For the purposes of describing the diffusion characteristics, these can be divided into five broad classes.

- One-dimensional (1D) channels: e.g. AFI, LTL, TON, CoFormate [20], MIL-47 [21], MIL-53(Cr) [22,23], Co(BDP) [24]; see Fig. 1.
- 1D channels with side pockets: e.g. MOR, FER; see Fig. 2.

* Corresponding author.
E-mail address: r.krishna@contact.uva.nl (R. Krishna).

http://dx.doi.org/10.1016/j.micromeso.2017.09.014
1387-1811/

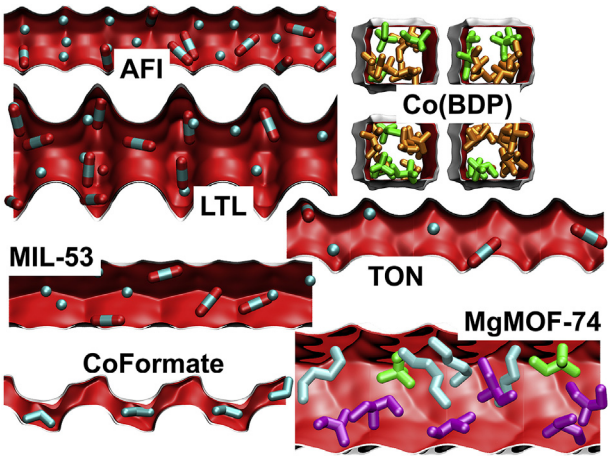

Fig. 1. Examples of one-dimensional (1D) channel structures: AFI, LTL, TON, MgMOF-74, MIL-53(Cr), and Co(BDP). We use iso-potential energy surfaces as representation of porous structures; we refer the reader to Keffer et al. [109] for an explanation of how these surfaces are to be interpreted.

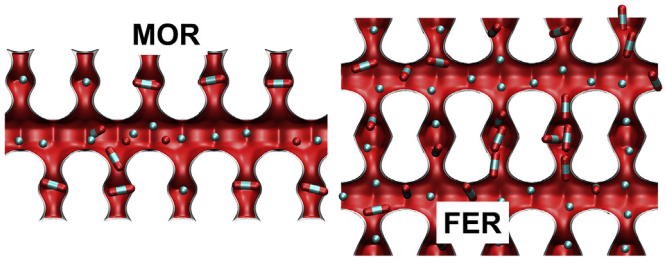

Fig. 2. Examples of 1D channel structures with side pockets: MOR and FER.

- Intersecting channels: e.g. MFI, BEA, ISV, Zn(bdc)dabco [25], Co(bdc)dabco [26]; see Fig. 3.
- Cages separated by narrow windows: e.g. AFX, LTA, CHA, DDR, TSC, ERI, ITQ-29, ZIF-8; see Fig. 4.
- Cavities with large windows: e.g. NaX, NaY, IRMOF-1 [27], CuBTC [28], MOF-177; see Fig. 5.

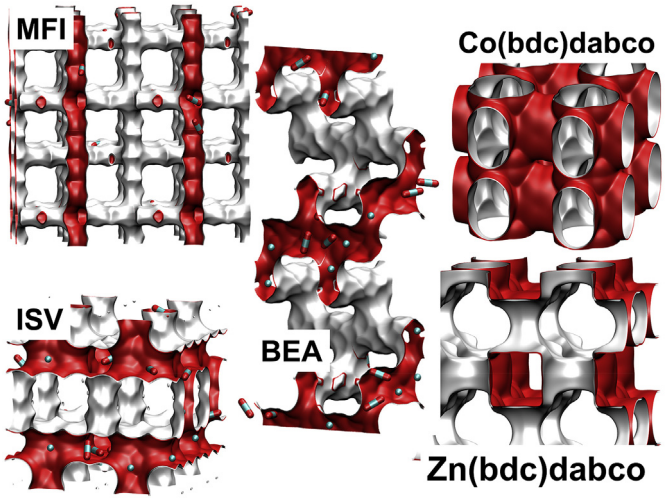

Fig. 3. Examples of structures consisting of intersecting channels: MFI, ISV, BEA, and Co(bdc)dabco, and Zn(bdc)dabco.

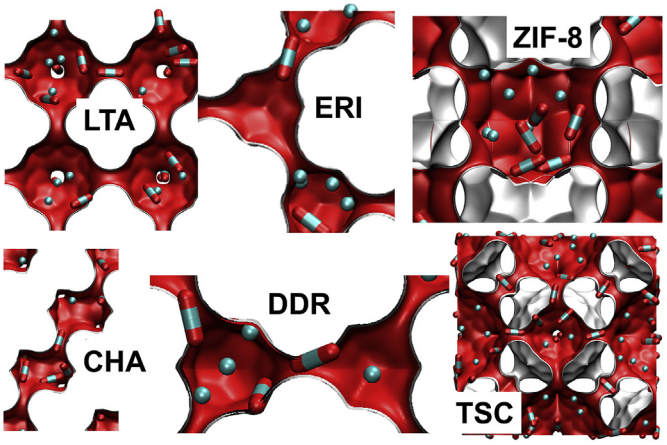

Fig. 4. Structures consisting of cages separated by narrow windows: LTA, CHA, DDR, ERI, TSC, and ZIF-8.

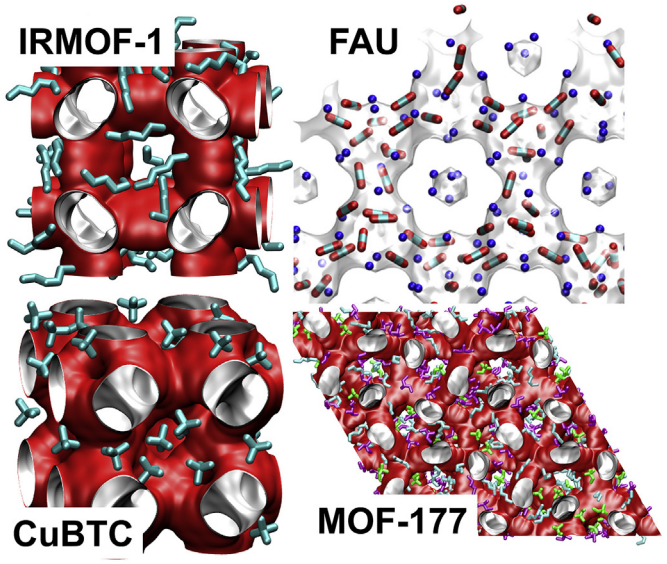

Fig. 5. "Open" structures that consist of cages separated by large windows: IRMOF-1, MOF-177, CuBTC, and FAU.

For zeolites, the crystallographic data are available on the zeolite atlas website of the International Zeolite Association (IZA) [29]. Further details on the structure, landscape, pore dimensions of a very wide variety of micro-porous materials are available in the published literature [16,30–36]. Generally speaking, the frameworks are not rigid. The zeolite framework flexibility is illustrated by animations of LTA-4A (see Video 1, uploaded as Supplementary Material), and LTA-5A (see Video 2). The consequences of framework flexibility for transport across 8-ring windows of LTA, CHA, DDR, and ERI have been investigated using molecular dynamics (MD) simulations [37–42]. Many MOFs possess soft "dynamic" frameworks whose cell dimensions change in a reversible manner to external stimuli [23,43–45]. Lattice flexibility of IRMOF-1 (see Video 3), that has large size cavities, has been found to increase the diffusivity by about 20%–50% [46]. It may be expected that lattice flexibility will have a greater influence when the molecule is more tightly constrained within a MOF framework. For ethane diffusion at high loadings in the 0.45 nm 1D channels of Zn(tbip), MD simulations have also shown that accounting for framework flexibility leads to diffusivity values that are about one order of magnitude

higher than for a fixed lattice [47]. The windows of ZIF-8 have a crystallographic dimension of 3.3 Å, but due to framework flexibility (see Video 4), even branched alkanes and aromatic molecules can hop across the windows [48,49]. The framework flexibility, and selective gate-opening of MOFs may be exploited to achieve industrially important separations [50,51].

Supplementary video related to this article can be found at http://dx.doi.org/10.1016/j.micromeso.2017.09.014.

To set the scene and define the objectives of this article, we consider seven experimental data sets on mixture diffusion; these data sets are representative of a much broader set of guest/host combinations.

For natural gas purification technologies using either LTA-4A or Ba-ETS-4 zeolites, the selective uptake of N_2 from CH_4, is a diffusion-selective process because the adsorption equilibrium favors CH_4 that has the higher polarizability [52–55]. For transient uptake of N_2/CH_4 mixtures, overshoots in the loading of the more mobile N_2 in LTA-4A zeolite have been reported in the classic paper by Habgood [52]; see Fig. 6. Analogously, the transient N_2/CH_4 uptake data of Majumdar et al. [54] for Ba-ETS-4 show overshoots in the uptake of the more mobile N_2. What is the root cause of the N_2 overshoot? How do we model N_2/CH_4 mixture uptake?

Zeolite membranes have potential use in a variety of separation applications [11,56,57]. In the majority of cases of industrial interest, the mixture permeation characteristics cannot be predicted solely on the basis of data on *unary* permeation of individual species in the mixture. As illustration, Fig. 7 compares the experimental data on permeances of CO_2 and H_2 determined for unary and binary mixture permeation across an MFI membrane [12]. The component permeances are defined by

$$\Pi_i \equiv \frac{N_i}{p_{i0} - p_{i\delta}} \tag{1}$$

where N_i represents the nolar fluxes across the membrane, and $p_{i0} - p_{i\delta}$ represents the differences in the partial pressures across the upstream ($z = 0$) and downstream ($z = \delta$) faces of the membrane.

The CO_2 and H_2 mixture permeances are both lower than the corresponding values for unary systems. For H_2, the lowering is by about one order of magnitude, while the CO_2 permeance is lowered by a factor of about two. This implies that mixture permeation is CO_2-selective, whereas the data based on unary permeation demonstrates H_2-selective performance. What causes the lowering of the component permeances in the mixture, and why is the extent of lowering significantly higher for H_2?

The alkylation of benzene to produce the industrially important ethylbenzene is carried out in fixed bed reactors using H-ZSM-5 as catalyst. H-ZSM-5 has the same topology as MFI, having intersecting channels of 5.5 Å size [58]. The catalyst effectiveness is strongly influenced by intra-crystalline diffusivity of ethene [5,59,60]. Hansen et al. [59] show that the effective diffusivity of C_2H_4 reduces significantly as the combined loading of benzene (Bz) and ethylbenzene (EthBz) in the catalyst increases to a value of 2 molecules per unit cell; see Fig. 8. What is the rationalization of the observed decrease of ethene diffusivity with (Bz + EthBz) loading?

In the PFG NMR studies of Förste et al. [61], the self-diffusivity of CH_4 in MFI is found to be significantly reduced as the loading of the co-adsorbed benzene increases to a value of about 2 molecules per unit cell; see Fig. 9a. In the PFG NMR investigation of Fernandez et al. [62], the self-diffusivity in MFI of n-butane (nC4), in mixtures with iso-butane (iC4), was found to decrease a few orders of magnitude as the loading of iC4 is increased from $\Theta_{iC4} = 0$ to 2 molecules per unit cell; see Fig. 9b. It is remarkable that three separate investigations (cf. Figs. 8 and 9) of mixture diffusion in MFI zeolite, find that the diffusivity of the more mobile guest molecules (respectively, C_2H_4, CH_4, and nC4) is reduced when the loading of the tardier partners (respectively, (Bz, and EthBz), Bz, and iC4) increases to a value of 2 molecules per unit cell. Can the three disparate set of experiments be rationalized on the same basis? If so, what is the explanation?

The selectivities for permeation of CO_2/CH_4, and C_2H_4/C_2H_6 mixtures across ZIF-8 membranes, for example, are dictated by a combination of diffusion and adsorption selectivities [16,56,63–67]. Fig. 10a and b show the experimental data of Chmelik et al. [68], obtained using Infra-Red Microscopy (IRM), on the effective Fick diffusivities, $D_{i,eff}$, of CO_2 and CH_4 in ZIF-8. For CO_2, the diffusivity in the CO_2/CH_4 mixture is practically the same as for the pure component; see Fig. 10a. On the other hand, the CH_4 diffusivity in the CO_2/CH_4 mixtures is significantly lower, by about one order of magnitude, than the unary diffusivity values; see Fig. 10b. Why is the diffusivity of CO_2 practically independent of

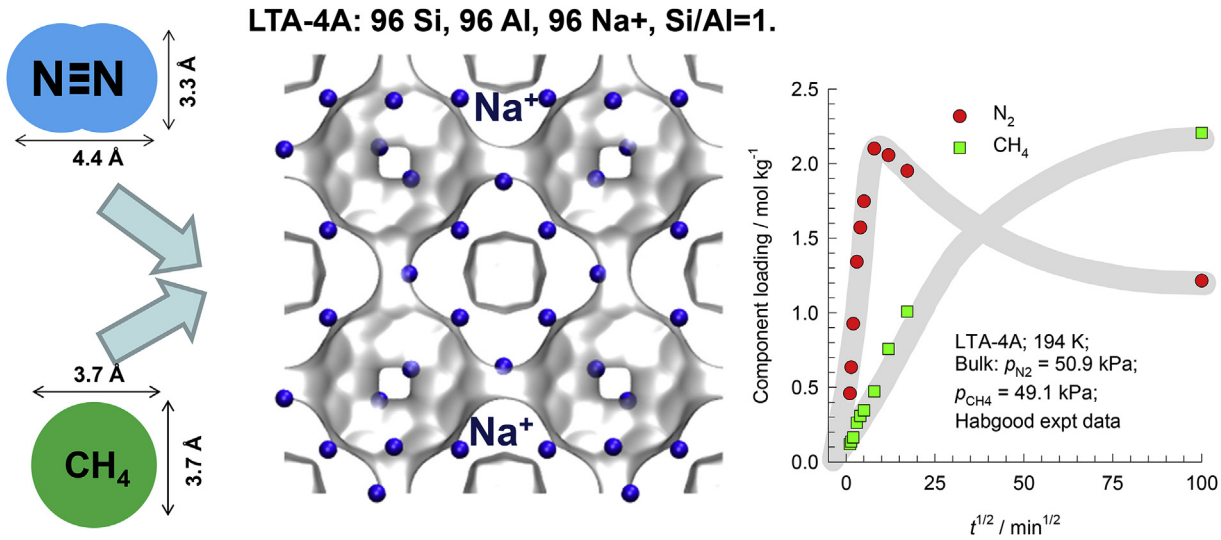

Fig. 6. Experimental data of Habgood [52] on transient uptake of $N_2(1)/CH_4(2)$ mixture within LTA-4A crystals, exposed to binary gas mixtures at 194 K and partial pressures $p_1 = 50.9$ kPa; $p_2 = 49.1$ kPa. The thick solid grey lines are "guides to the eye".

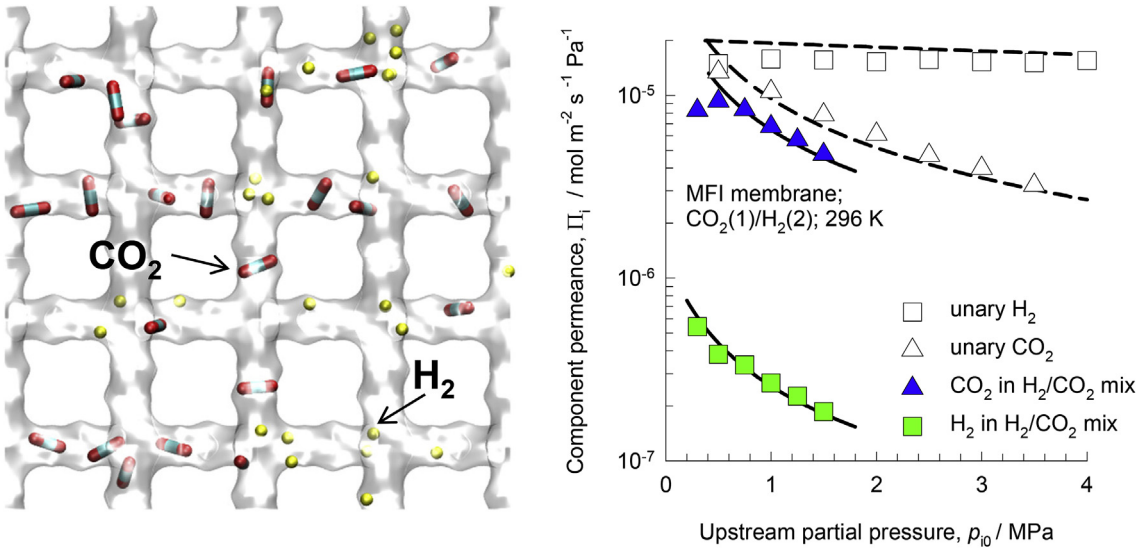

Fig. 7. Snapshots showing the location of CO_2, and H_2 within the intersecting channels of MFI zeolite. Experimental data [12] for the permeances of CO_2(1) and H_2(2) determined for unary and binary CO_2(1)/H_2(2) mixture permeation across MFI membrane at 296 K. The data are plotted as a function of the partial pressure of CO_2 (= H_2) in the upstream compartment. The dashed lines are fits of unary permeances. The continuous solid lines are model calculations [16,66,67] using the Maxwell-Stefan diffusion model.

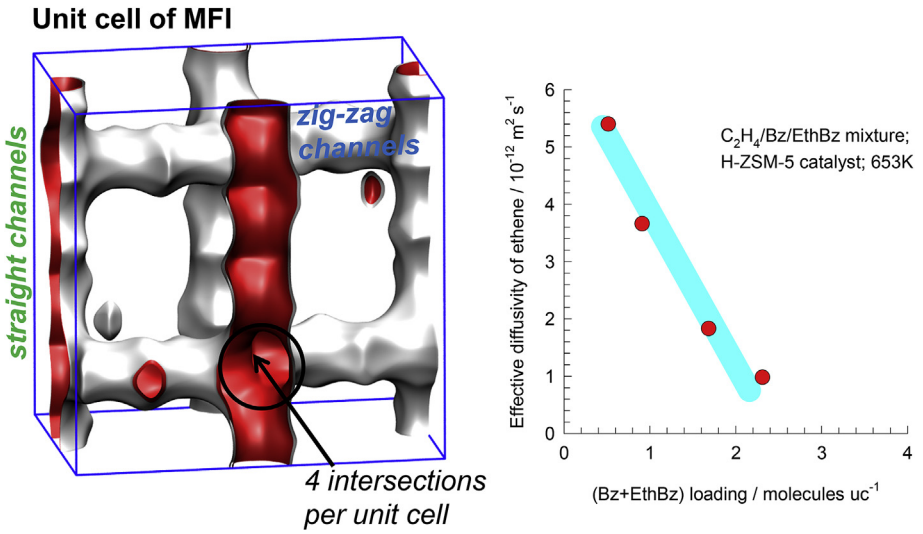

Fig. 8. (a) Snapshots showing the location of ethene, benzene, and ethylbenzene within the intersecting channel topology of MFI zeolite. (b) The effective diffusivity of ethene within H-ZSM-5 catalyst is plotted as a function of the (Benzene + Ethylbenzene) loading in the mixture [59]. The thick solid cyan line is "guide to the eye". (For interpretation of the references to colour in this figure legend, the reader is referred to the web version of this article.)

mixture composition, whereas the diffusivity of CH_4 in the mixture falls significantly below the corresponding unary diffusivity values?

For water/N-methylpyrrolidone (NMP) pervaporation across CHA membrane, operated on an industrial scale, the NMP permeance shows a decreasing trend with increasing feed water composition; see Fig. 11. Correspondingly, the water permeance decreases with increasing proportion of NMP in the feed mixture. The mutual diminishing influences on component permeances are not easy to rationalize on the basis of simple Fickian models of intra-crystalline diffusion; how do we explain these experimental findings?

The primary objective of this article is to seek explanations and rationalization of the experimental results presented in Figs. 6–11. Towards this end, we use Molecular Dynamics (MD) simulation data, along with video animations portraying the molecular traffic within a variety of microporous materials, to provide fundamental insights, that will assist in setting up the proper phenomenological models to be used in the design of pressure swing adsorbers, catalytic reactors, and membrane separation devices. Details of molecular simulation techniques are not provided in this article; the reader is referred to reviews [31,69–72] and texts [73,74].

2. Slowing-down effects in microporous channels

The guest molecules in microporous materials exist in the adsorbed phase. The mobilities of the guest molecules are significantly influenced by their respective adsorption strengths. Generally speaking, the more strongly adsorbed species has a lower mobility, because it "sticks" to the pore walls more strongly [32,34]. For operations of separation and reaction processes at reasonably high pore occupancies, the molecular jumps, and hops, of the guest species are *correlated*, because the component with the higher

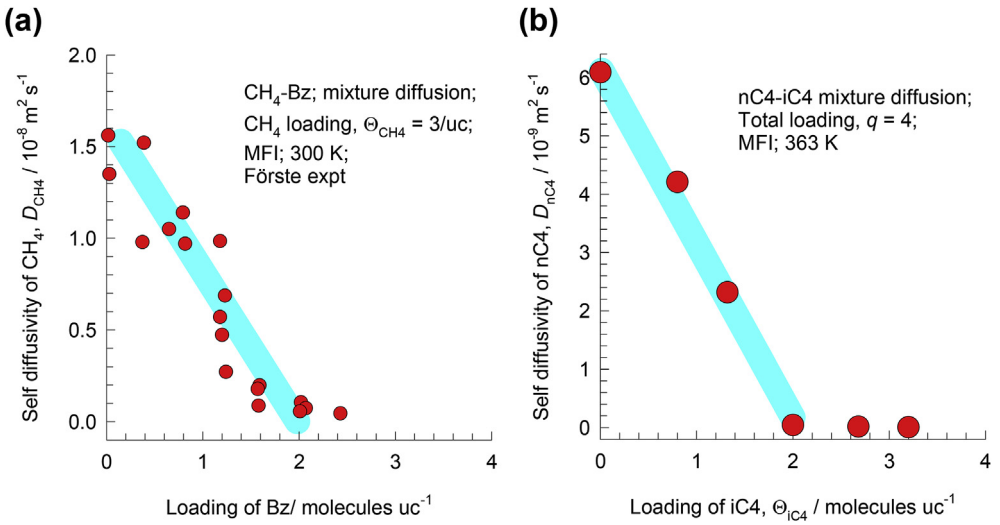

Fig. 9. (a) PFG NMR experimental data [61] on self-diffusion coefficients of CH_4 in CH_4/Benzene mixtures in MFI zeolite as a function of the loading of Benzene in the mixture. The methane loading in the experiments is $\Theta_{CH4} = 3$ uc^{-1}. (b) PFG NMR experimental data [62] on self-diffusion coefficients of n-butane (nC4) in n-butane (nC4)/iso-butane (iC4) mixtures in MFI as a function of the loading of iC4. The total loading in the experiments is $\Theta_t = 4$ uc^{-1}. The thick solid cyan lines are "guides to the eye". (For interpretation of the references to colour in this figure legend, the reader is referred to the web version of this article.)

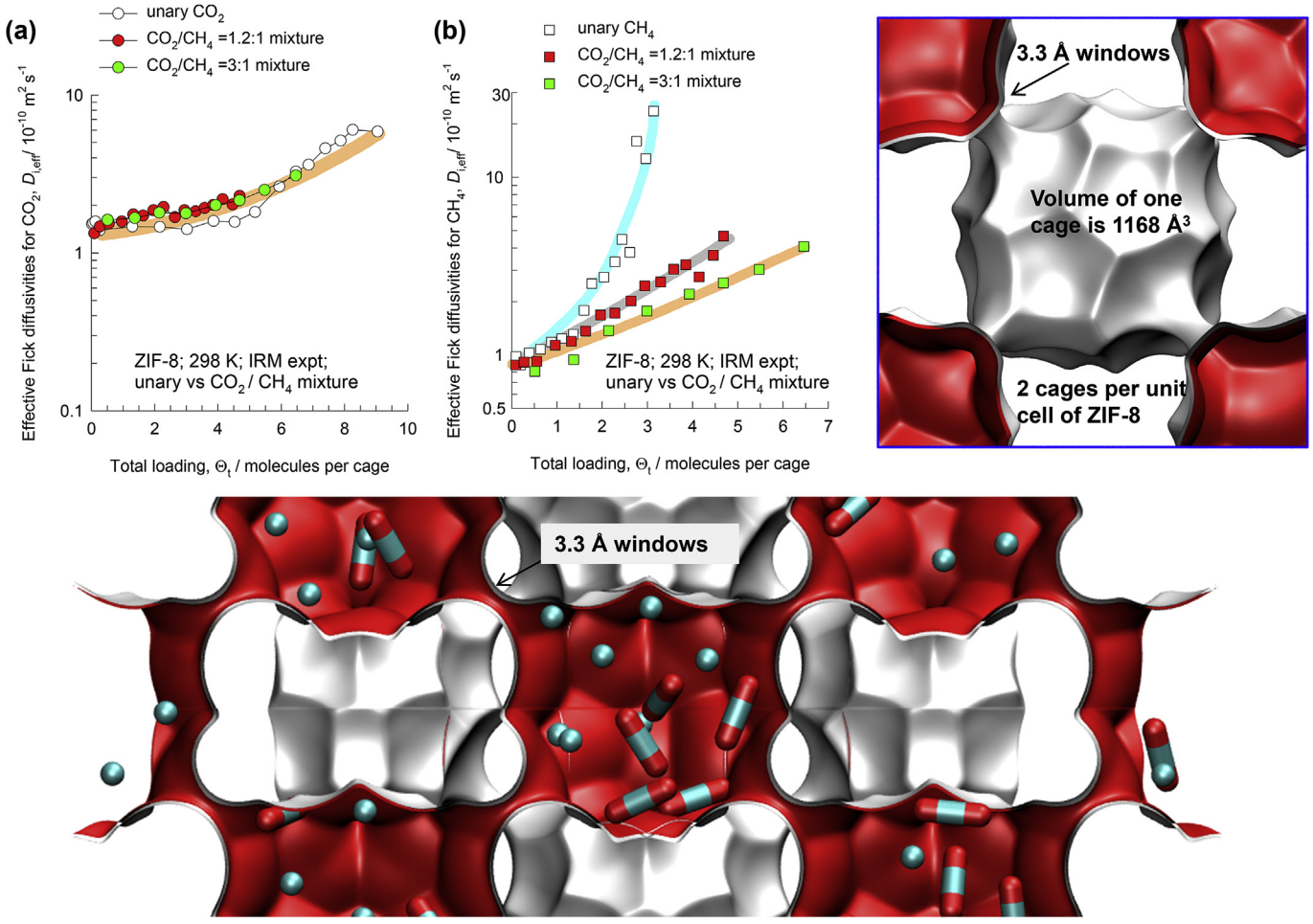

Fig. 10. (a, b) Effective Fick diffusivities, $D_{i,eff}$, of individual components in mixtures of (a) CO_2 and (b) CH_4 in ZIF-8 crystal as a function of the total mixture loading, Θ_t. The values for two different CO_2/CH_4 loadings within the crystal, 3:1, and 1.2:1, are compared to the unary Fick diffusivities, D_i. The mixture experiments were carried out with constant gas phase compositions with CO_2/CH_4 ratios of 1.13 and 2.86, respectively. The data presented in this Figure are taken from Chmelik et al. [68] The thick solid lines are "guides to the eye".

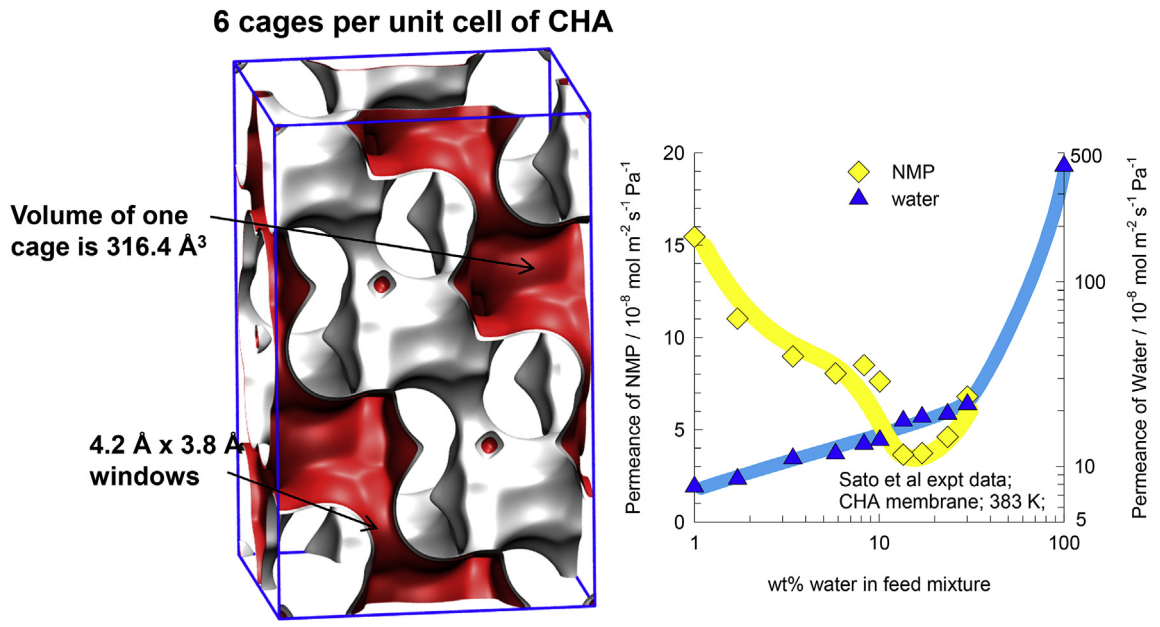

Fig. 11. Permeances of water and NMP across for water/NMP pervaporation across CHA membrane [110]. The thick solid lines are "guides to the eye".

adsorption strength (i.e. the tardier species) needs to vacate an adsorption site before that site can be occupied by the component with the lower adsorption strength (i.e. the more mobile component). Generally speaking, the mobility of the more mobile species is lowered due to *correlated jumps* with the tardier partner molecules. Such *slowing-down* effects can be appreciated by examination of a few animations of mixture diffusion. For CO_2/H_2 mixture diffusion in the 1D channels of TON zeolite, the more mobile H_2 suffers significant slowing-down by the more strongly adsorbed CO_2; see Video 5. Similarly, the tardier CO_2 exerts a retarding influence on the more mobile CH_4 partner molecules for CO_2/CH_4 mixture diffusion in the 1D channels of AFI zeolite; see Video 6. For CO_2/H_2 separations with MgMOF-74 membranes, the permeation selectivity is in favor of CO_2, because of two separate reasons [75]: (1) the adsorption favors CO_2, and (2) the more mobile H_2 is slowed-down due to correlation effects in the hexagonal shaped 11 Å channels; see Video 7. For propene/propane diffusion in the 11 Å hexagonal channels of FeMOF-74 [9,76], the more strongly adsorbed propene has a slowing-down on the more mobile propane molecules; see Video 8, and Video 9. Within the intersecting channels of MFI, the more strongly adsorbed CO_2 has a significant retarding influence on the mobility of the more mobile CH_4 (see Video 10) and H_2 (see Video 11).

Supplementary video related to this article can be found at http://dx.doi.org/10.1016/j.micromeso.2017.09.014.

The two sets of MD simulations presented in Fig. 12a and b provide quantitative evidence of slowing-down effects for CO_2/H_2 mixture diffusion in MFI zeolite. In Fig. 12a, the MD simulations of the self-diffusivities are plotted as a function of the total mixture loading, q_1+q_2, keeping $q_1 = q_2$. We note that the diffusivity of H_2 is significantly reduced, by about an order of magnitude, at increased mixture loadings. In Fig. 12b, the MD simulation data are obtained at a constant total loading, $q_1+q_2 = 1.734$ mol kg^{-1}, and the fraction of CO_2 in the adsorbed phase is varied from 0 to 1. With increasing proportion of the tardier CO_2 in adsorbed phase, the diffusivity of H_2 is progressively reduced by about an order of magnitude. The MD data in Fig. 12a and b explain the significant reduction in the H_2 permeance for mixture permeation across MFI membranes as witnessed in Fig. 7. The quantitative modelling of the slowing-down effects in membrane permeation requires use of the Maxwell-Stefan diffusion formulation [16,66,67]. For CH_4/C_2H_6, and CH_4/C_3H_8 mixture diffusion in MFI zeolite, the longer alkane exercises a retarding influence on the mobility of the more mobile methane; see Video 12, and Video 13; such slowing-down effects need to be accounted for in modelling the experimental data of van der Graaf et al. [77].

Supplementary video related to this article can be found at http://dx.doi.org/10.1016/j.micromeso.2017.09.014.

3. Traffic junction effects in MFI zeolite

Configurational-Bias Monte Carlo (CBMC) simulations of the unary adsorption isotherms for linear alkanes, with carbon numbers ranging from 1 to 6 in MFI zeolite at 300 K are shown in Fig. 13a. The linear alkanes can locate anywhere along the straight channels and zig-zag channels, and there are no perceptible isotherm inflections. The intersections between the straight channels and zig-zag channels of MFI zeolite act like traffic junctions; there are 4 intersections per unit cell. Due to configurational restraints, branched alkanes prefer to locate at the channel intersections because of the extra "leg room" that is available here. An extra "push" is required to locate these molecules within the channel interiors. This extra push results in an inflection in the pure component isotherms at a loading of 4 molecules per unit cell [78–81]; see CBMC simulation data for iso-butane (iC4), 2-methylpentane (2MP), and 2,2dimethylbutane (22DMB) in Fig. 13b. Cyclic hydrocarbons, such as cyclohexane, Benzene (Bz), and ethylbenzene (EthBz) also prefer to locate at the intersections; the unary isotherm for benzene also exhibits a strong inflection at a loading, $\Theta = 4$ molecules per unit cell. Video animations, created from MD simulations of unary diffusion of nC4 (Video 14), iC4 (Video 15), benzene (Video 16), and cyclohexane (Video 17) are provided as Supplementary Materials. These animations demonstrate that the branched iC4 appears to be practically stagnant at the intersection location, for the duration of the MD simulations. The cyclic hydrocarbons benzene and cyclohexane exhibit rotational motion, but do not appear to move between intersections for the duration time of the MD simulations. The relative stagnancy of

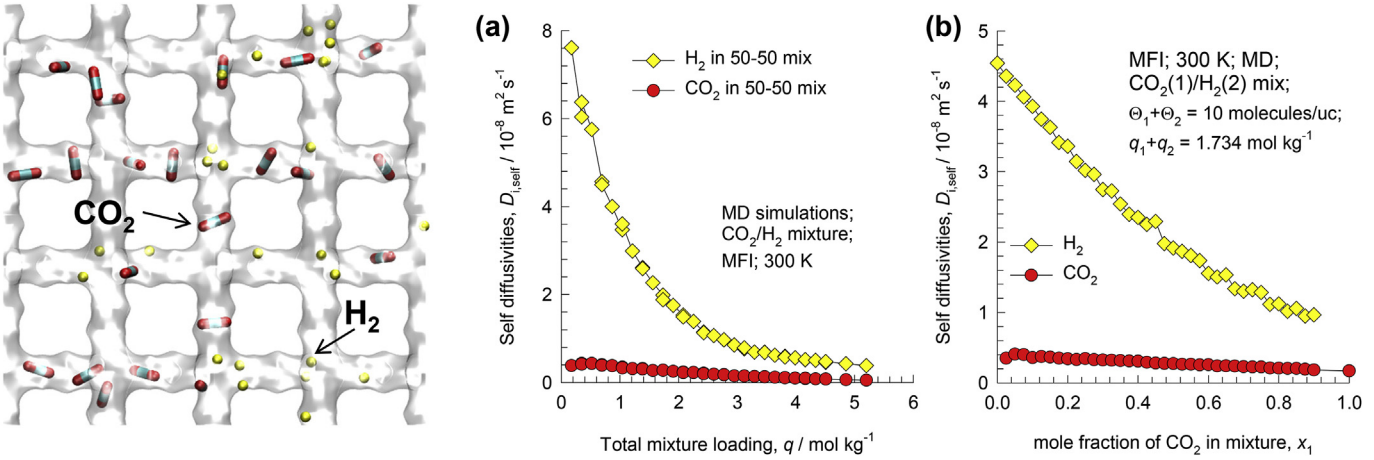

Fig. 12. (a, b) MD simulations of the self-diffusivities of CO_2, and H_2 for $CO_2(1)/H_2(2)$ mixtures within the intersecting channels of MFI zeolite at 300 K. In (a) the self-diffusivites are plotted as a function of the total mixture loading, q_1+q_2, keeping $q_1 = q_2$. In (b) the total loading is held constant at $q_1+q_2 = 1.734$ mol kg^{-1}, and the fraction of CO_2 in the adsorbed phase is varied from 0 to 1.

these molecules is tantamount to obstruction, and hindering, of free traffic of partner molecules such as linear alkanes and alkenes. This can be discerned in the animations of binary diffusion of nC4/iC4 mixtures at a total loading of 4 molecules per unit cell; see Video 18, Video 19, and Video 20.

Supplementary video related to this article can be found at http://dx.doi.org/10.1016/j.micromeso.2017.09.014.

The MD simulated values of the self-diffusivities of nC4 in nC4/iC4 mixture are plotted as a function of the iC4 loading in Fig. 14b. The MD data are in qualitative agreement with the corresponding experimental data in Fig. 9b. The reason for this strong decline in the nC4 diffusivity can be understood on the basis of the preferential location of iC4 at the channel intersections of MFI. For $\Theta_{iC4} = 2$, half the total number of intersections are occupied by iC4, that has a diffusivity which is about three orders of magnitude lower than that of nC4. Since the occupancy of the intersections is distributed randomly, each of the straight channels has an iC4 molecule ensconced somewhere along the channels; this is evident from the snapshot in Fig. 14a. This is tantamount to blockage and leads to severe reduction in the molecular traffic of the intrinsically more mobile nC4. Uptake experiments of Chmelik et al. [82] provide further evidence of the influence exerted by iC4 on co-diffusion of nC4 in MFI crystals.

The important message emerging from the MD data in Fig. 14 is that it is only necessary for half of the intersection sites to be "blocked" by iC4 in order to bring the nC4 traffic to a virtual halt. This explanation and conclusion also holds equally well for CH_4/benzene mixture diffusion; see MD simulated self-diffusivities in Fig. 15. The MD simulated self-diffusivity of CH_4 shows precisely the same trend as evidenced in the Förste et al. [61] experiments shown in Fig. 9a. The blocking of methane traffic by benzene molecules that occupy the intersection sites can be ascertained in Video 21.

Supplementary video related to this article can be found at http://dx.doi.org/10.1016/j.micromeso.2017.09.014.

Fig. 16 shows the MD simulated data on the self-diffusivity of C_3H_6 in C_3H_6/benzene mixtures; the observed trends are analogous to experimental data in Fig. 8, as reported by Hansen et al. [59]. Both benzene (reactant) and ethylbenzene (product) are preferentially located at the intersections of MFI; see Fig. 16c. The blocking of intersections by the aromatic molecules causes effective diffusivity of ethene inside the catalyst to reduce five-fold as the loading of benzene and ethylbenzene approaches two molecules per unit cell. The proper incorporation of traffic junction effects is essential in the quantitative modeling of catalyst effectiveness, as has demonstrated by Hansen et al. [59].

Schuring et al. [83] have reported experimental data on the self-diffusivities of both n-hexane (nC6) and 2-methylpentane (2MP) in nC6/2MP mixtures. These measurements were made at a total loading $\Theta_t = 3.5$ molecules uc^{-1}. Their data, plotted in Fig. 17a, shows that *both* self-diffusivities are reduced with increasing loading of 2MP in the mixture. The preferential location of 2MP at the intersections causes blocking of nC6 traffic in the intersecting channel system of MFI; this blocking of nC6 traffic by 2MP can be identified by viewing Video 22, and Video 23.

Supplementary video related to this article can be found at http://dx.doi.org/10.1016/j.micromeso.2017.09.014.

Titze et al. [84] report the Maxwell-Stefan diffusivity values, $Đ_1/r_c^2$, and $Đ_2/r_c^2$ that are fitted to match experimental data on four sets of experiments for uptake of nC6/2MP mixtures in MFI zeolite crystals; see Fig. 17b. The diffusivities of both nC6 and 2MP decrease strongly with increased 2MP loading, precisely analogous to that observed by Schuring et al. [83]. Clearly, intersection blocking effects are also in play here. We also note a further characteristic for this mixture of more-mobile-more-strongly-adsorbed-nC6 and tardier-less-strongly-adsorbed-2MP. There is uncommon synergy because both adsorption and diffusion favor the linear isomer [84].

4. Inter-cage hopping of molecules in cage-type zeolites

In order to rationalize the N_2 overshoot during transient uptake of N_2/CH_4 mixtures in LTA-4A, we need insights into both adsorption and diffusion characteristics. LTA-4A zeolite consists of cages of 743 Å^3 volume that are separated by 8-ring windows of 4.1 Å × 4.4 Å size; see pore landscape in Fig. 6, and snapshots of guest molecules in Fig. 18a. Each unit cell LTA-4A has 96 Si, 96 Al, 96 Na^+, with Si/Al = 1. CBMC simulations of the unary isotherms (cf. Fig. 18b), show that CH_4 has an adsorption strength that is about a factor 2–3 times higher than that of N_2; this is ascribable to the higher polarizability of methane. Both N_2 and CH_4 jump one-at-a-time across the 4.1 Å × 4.4 Å windows, i.e. the jumps are practically uncorrelated [38,65,85]. The one-at-a-time hopping of molecules across the windows are best appreciated by viewing Video 24, and Video 25. The animations show that the 3.3 Å × 4.4 Å sized pencil-like N_2 molecules jumps length-wise across the windows. Since the cross-sectional dimension of N_2 molecule is smaller than that of CH_4, we should expect N_2 to have a higher inter-cage

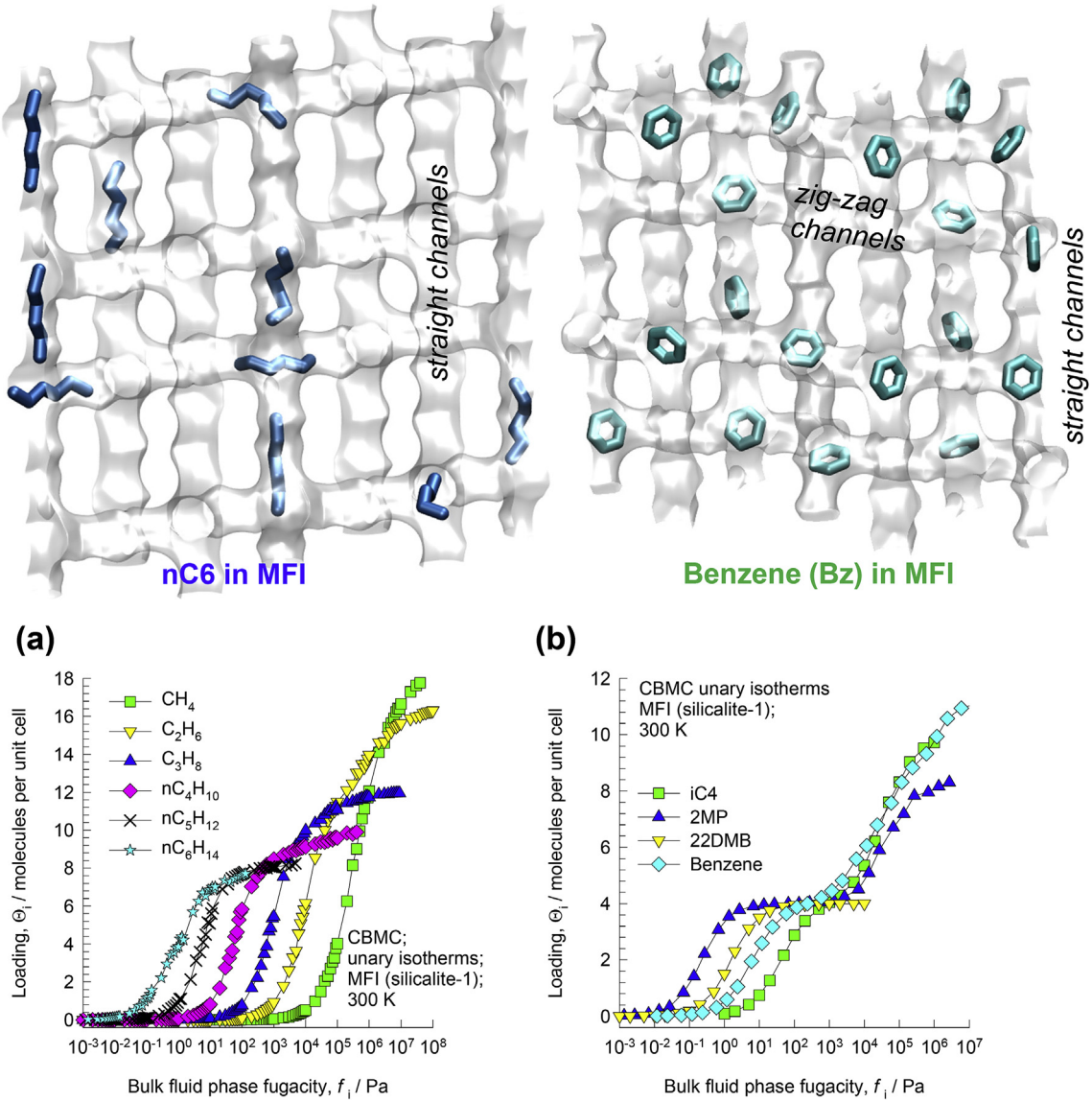

Fig. 13. (a) CBMC simulations for linear alkanes, with carbon numbers ranging from 1 to 6 in MFI zeolite at 300 K. (b) CBMC simulations for branched alkanes and benzene in MFI zeolite at 300 K.

diffusivity. Molecular dynamics simulations of unary diffusivities (cf. Fig. 18c) show that the diffusivity of N_2 is about a factor 20 to 50 higher than that of CH_4. The transient uptake of mixtures containing more-mobile-less-strongly-adsorbed components and tardier-more-strongly adsorbed partners, usually exhibits overshoots in the uptake of the more mobile species [55]. For example, Binder et al. [86] and Lauerer et al. [87] report overshoots in the loading of CO_2 during uptake of CO_2/C_2H_6 mixtures in DDR cage-type zeolite. A detailed examination of the origins of such overshoots [55], reveals that they are engendered by thermodynamic coupling between species transfers.

Supplementary video related to this article can be found at http://dx.doi.org/10.1016/j.micromeso.2017.09.014.

5. Hindered hopping of molecules across windows of cage-type zeolites and ZIFs

For separation of CO_2 from gaseous mixtures with CH_4, and N_2, cage-type materials such as DDR, CHA, LTA, ERI, and ZIF-8 are of practical interest; these materials consist of cages separated by narrow windows, in the 3.3–4.5 Å range. The selectivity of separation of CO_2 is dictated by both adsorption and diffusion characteristics. For adsorption of CO_2/CH_4 mixtures, CBMC simulations [88] show that the window regions of cage-type zeolites has a significantly higher proportion of CO_2 than within the cages; the preferential location of CO_2 has important consequences in mixture diffusion.

Fig. 19b–d show the data on self-diffusivities in CO_2/CH_4, CO_2/N_2, and CO_2/Ar mixtures in DDR at a fixed value of total loading $q_t = 2.77$ mol kg^{-1}, and varying composition of the adsorbed mixtures. For all three mixtures, increasing the proportion of the adsorbed phase composition of CO_2 has the effect of reducing the diffusivity of the partner molecules, CH_4, N_2, and Ar. This reduction is directly ascribable to the preferential perching of CO_2 at the window regions. The windows of DDR are 3.65 Å × 4.37 Å; the dimensions of a CO_2 molecule are 5.5 Å × 3.1 Å (see Fig. 19), and therefore CO_2 can only jump lengthwise across the windows of DDR. Simply put, CO_2 hinders the inter-cage hopping of its partner

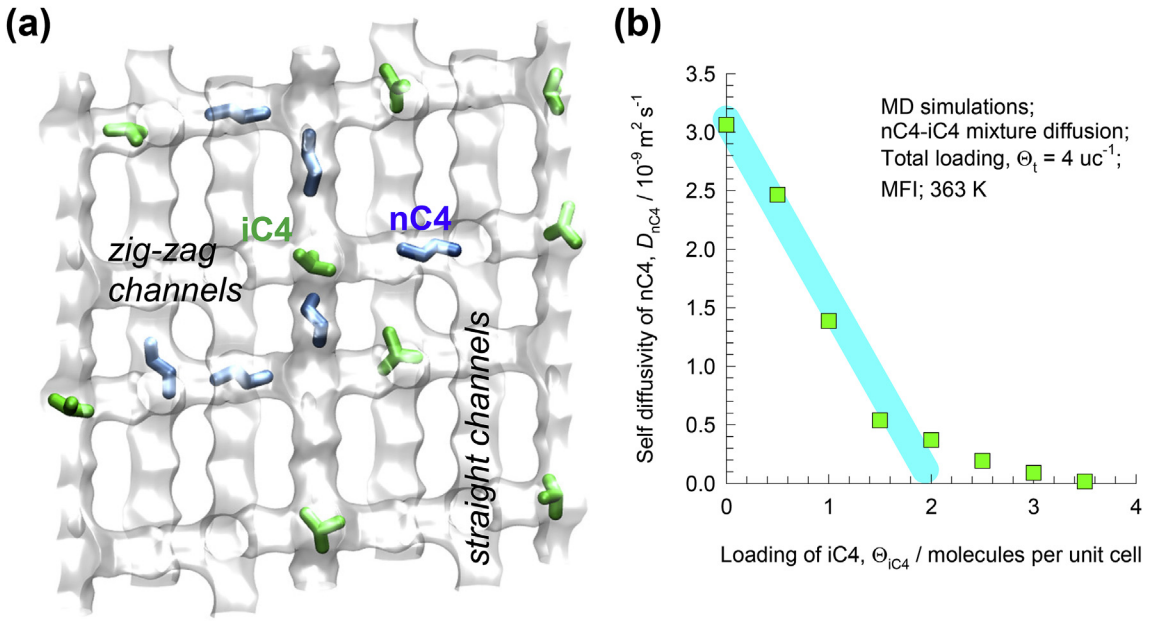

Fig. 14. (a) Snapshots showing the location of nC4 and iC4 within the intersecting channels of MFI zeolite. The total mixture loading, $\Theta_t = 4$ uc^{-1}. (b) MD simulations [62] for self-diffusivities of nC4 in nC4)/iC4 mixtures in MFI at 363 K as a function of the iC4 loading in the mixture; the total mixture loading is maintained constant at $\Theta_t = 4$ uc^{-1}. The thick solid cyan line is "guide to the eye". (For interpretation of the references to colour in this figure legend, the reader is referred to the web version of this article.)

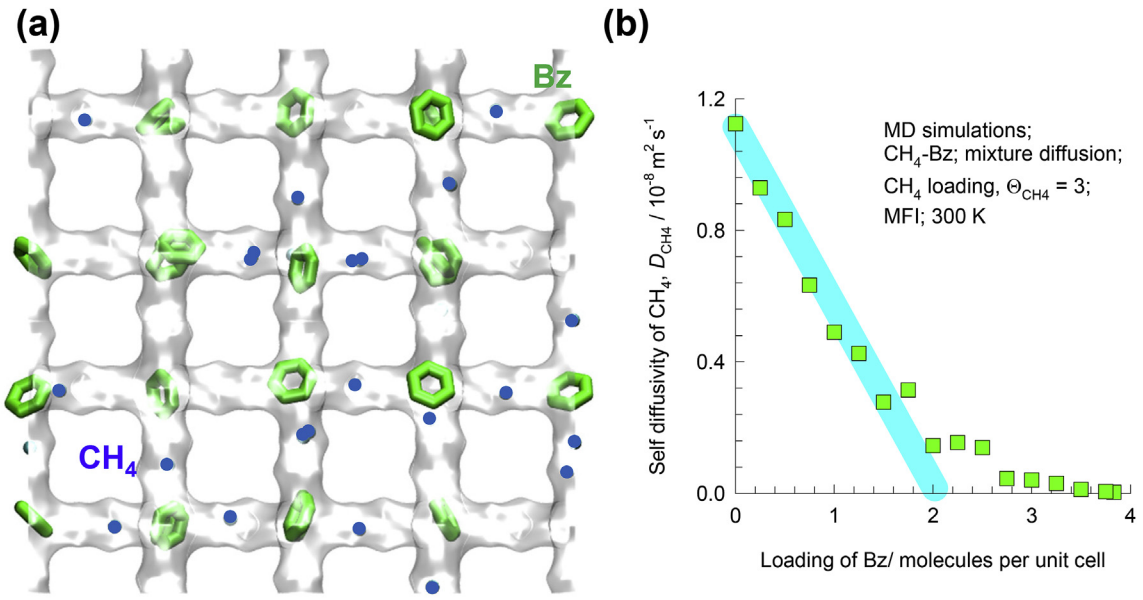

Fig. 15. Snapshots showing the location of CH_4 and Bz within the intersecting channels of MFI zeolite. The total mixture loading, $\Theta_t = 4$ uc^{-1}. MD simulations [111] for self-diffusivities of CH_4 in CH_4/Bz mixtures in MFI at 300 K as a function of the Bz loading in the mixture; the total CH_4 loading is maintained constant at $\Theta_{CH4} = 3$ uc^{-1}. The thick solid cyan line is "guide to the eye". (For interpretation of the references to colour in this figure legend, the reader is referred to the web version of this article.)

molecules; this hindering effect due to location of CO_2 at windows of DDR can be discerned by viewing Video 26. Such hindering effects need to be taken into account in order to interpret experimental data for CO_2/CH_4 permeation experiments across DDR membranes [89,90]. Fig. 20 compares the membrane transport coefficients, $(\rho Đ_i/\delta)$, for CO_2, and CH_4, backed out from unary and binary mixture permeation data across DDR membrane. The transport coefficient for CO_2 in the mixture is the same as that determined from unary permeation experiments, when compared at the same mixture loading, Θ_t. In sharp contrast, there is a dramatic reduction in the transport coefficient of CH_4 in the mixture, especially at higher loadings, when compared to the data from unary permeation; consequently the permeance of CH_4 in the mixture is significantly lower than that of the pure component. It must be emphasized that the reduction of the transport coefficient of CH_4 is *not* ascribable to correlation effects; such effects lower the mobility of the *more mobile partner* species [66,75]. The reduction of the mobility of tardier CH_4 in the mixture is a consequence of the blocking of window regions due to preferential location of CO_2 molecules. For DDR, window blocking by CO_2 is desirable in practice because the membrane permeation selectivities will be significantly enhanced above the values anticipated on the basis of pure component permeances.

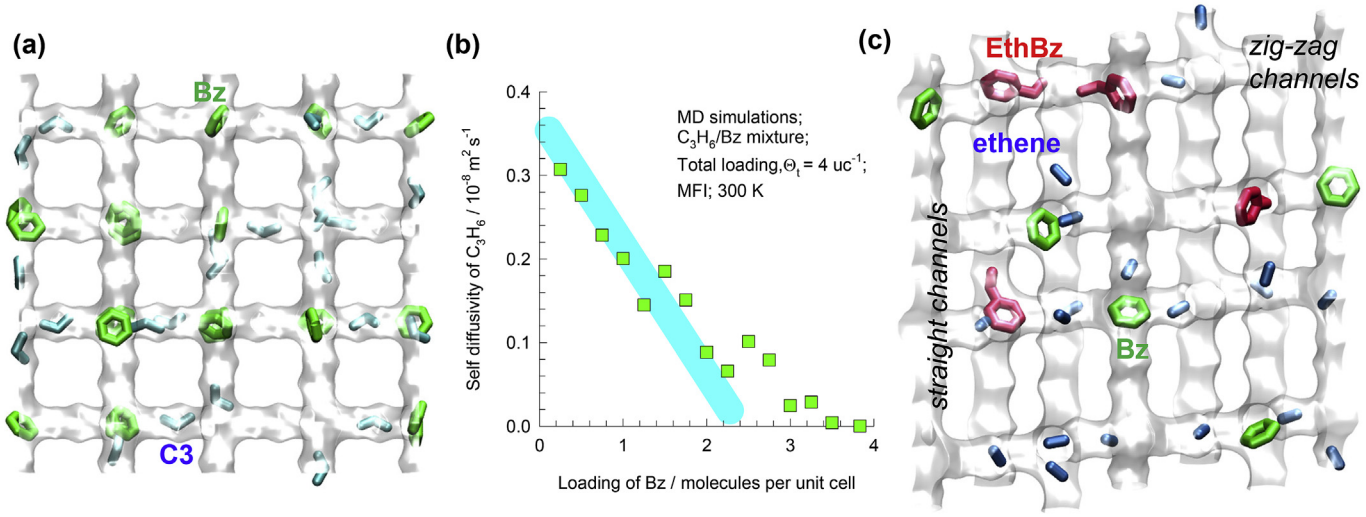

Fig. 16. (a) Snapshots showing the location of C3 and benzene in MFI zeolite (b) MD simulations [111] for self-diffusivities of C_3H_6 in C_3H_6/Bz mixtures in MFI at 300 K as a function of the Bz loading in the mixture; the total mixture loading is maintained constant at $\Theta_t = 4$ uc^{-1}. The thick solid cyan line is "guide to the eye". (c) Snapshot showing the location of reactants and products in the alkylation of benzene with ethene to produce ethylbenzene within the intersecting channel topology of MFI catalyst. (For interpretation of the references to colour in this figure legend, the reader is referred to the web version of this article.)

Supplementary video related to this article can be found at http://dx.doi.org/10.1016/j.micromeso.2017.09.014.

The preponderance of CO_2 molecules at the window regions also manifests for ZIF-8, as evidenced in the probability density plots presented in the publication of Chmelik et al. [68]. The IRM experimental data in Fig. 10b and c are precisely analogous to the data on transport coefficients, $(\rho \mathcal{D}_i/\delta)$ defined in terms of the Maxwell-Stefan diffusivities, in the DDR membrane shown in Fig. 20. The experimental data in Fig. 10b can be rationalized by analogous reasoning to that for DDR membrane; the Fick diffusivity of CH_4, defined in terms of the gradients of molar loadings, is suppressed due to hindering by CO_2 molecules located at the window regions. A qualitative appreciation of CO_2/CH_4 mixture diffusion in ZIF-8 is obtained by viewing Video 27.

Supplementary video related to this article can be found at http://dx.doi.org/10.1016/j.micromeso.2017.09.014.

6. Mutual slowing-down due to hydrogen bonding

For diffusion of mixtures containing water and alcohol, the formation of O···H ("hydrogen bonds") between water-water, water-alcohol, and alcohol-alcohol pairs has a significant impact on adsorption and diffusion characteristics [91–93]. The formation of O···H bonds between molecular pairs causes formation of clusters. A molecular cluster can be regarded as a *k*-mer; for example a dimer. One characteristic signature of cluster formation is that the adsorption isotherm exhibits a steep increase in the loading, the inverse thermodynamic factor $\frac{1}{\Gamma} = \frac{f}{\Theta}\frac{\partial \Theta}{\partial f}$ exceeds unity, i.e.: $\frac{1}{\Gamma} > 1$, for a range of pore concentrations; here f is the bulk fluid phase fugacity, and Θ is the molar loading. The inverse thermodynamic factor has the physical significance of fractional *vacancy* in the pores. Fig. 21a shows calculations of the inverse thermodynamic factor for methanol and ethanol adsorption within the cages of ZIF-8. A *k*-mer occupies nearly the same vacant adsorbed site as a normal, unclustered, molecule, and the fractional vacancy can exceed unity [91,92]. A visual indication of methanol, and ethanol clustering in ZIF-8 is provided by the snapshots in Fig. 21, along with the animations in Video 28, and Video 29. In concentration regions where $\frac{1}{\Gamma} > 1$, an increase in the molar loading leads to a decrease in the unary diffusivity; see experimental data of Chmelik et al. [94] plotted in Fig. 21b and c. The unusual loading dependence of the unary diffusivities is directly ascribable to molecular clustering.

Supplementary video related to this article can be found at http://dx.doi.org/10.1016/j.micromeso.2017.09.014.

For adsorption of methanol/ethanol mixtures in FER zeolite, Fig. 22a presents data on the radial distribution functions (RDFs) for distances between all combinations of O and H atoms of molecule pairs. For all three molecular pairs, the first peaks manifest at distances smaller than 2 Å; this distance is characteristic of H-bonding [95]. The H-bonding of the methanol-methanol pair is strongest as the peak height is the highest. An important consequence of H-bonding between methanol and ethanol is that the molecular clusters formed will move in consort. Fig. 22b shows the MD simulations of the self-diffusivities of methanol and ethanol in mixtures of different compositions. The self-diffusivities are close together, and the differences are less than a factor of two. Some evidence of the influence of H-bonding on diffusivities of methanol/ethanol mixtures in FER can be gleaned from data in Kärger et al. [96] obtained from micro-imaging techniques.

For water/alcohol mixture diffusion in zeolites, MOFs, and ZIFs, the diffusivity of each component is lowered significantly due to H-bonding [92,97–99]. The formation of molecular clusters is demonstrated in Video 30, Video 31, and Video 32. Fig. 23 presents MD simulations of self-diffusivities for water/methanol, and water/ethanol mixtures in FAU, DDR, and CHA zeolites. In all cases, the diffusivity of water is reduced with increasing proportion of alcohol. Concomitantly, the diffusivity of the alcohol is diminished for a range of water compositions in the adsorbed phase. Hydrogen bonding between water and alcohol molecule pairs serves to act as a "flexible leash" linking the motion of the more mobile (water) and tardier (alcohol) species. The net result is that the motion of water is retarded due to cluster formation; the leash also serves to reduce the mobility of the alcohol molecules.

Supplementary video related to this article can be found at http://dx.doi.org/10.1016/j.micromeso.2017.09.014.

The experimental data on water/NMP pervaporation across CHA membrane (cf. Fig. 11) can be explained on the basis of mutual-slowing down caused by molecular clustering. For water/alcohol pervaporation across CHA zeolite membrane, the experimental

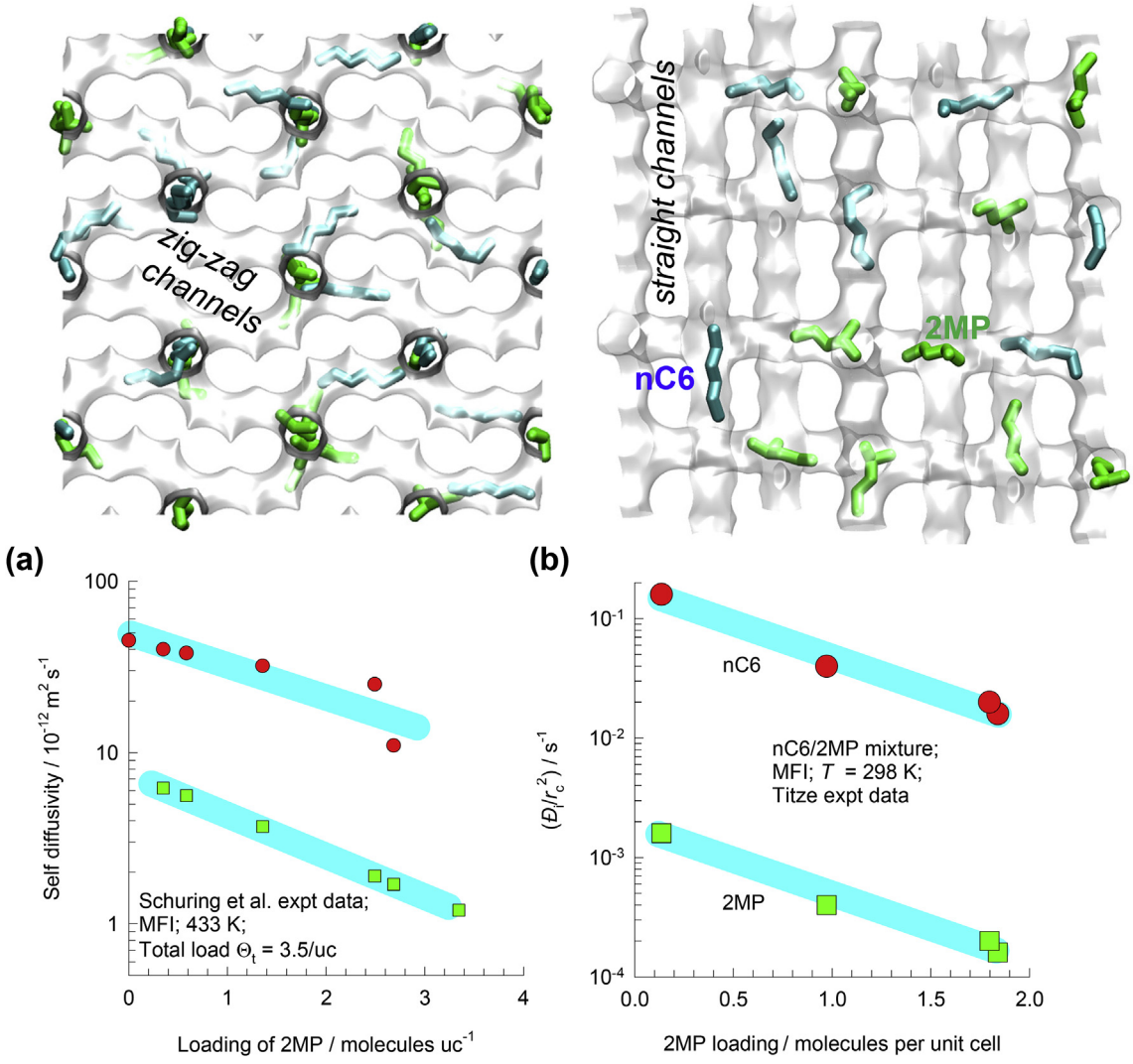

Fig. 17. (a) Experimental data [83] on self-diffusivities of nC6 and 2-methylpentane (2MP) as a function of the loading of 2MP, keeping the total loading $\Theta_t = 3.5$/uc. (b) Values of the fitted Maxwell-Stefan diffusivities, $Đ_1/r_c^2$, and $Đ_2/r_c^2$ for nC6 (1) and 2MP (2) chosen to match the four sets of experimental nC6(1)/2MP(2) uptake data of Titze et al. [84], plotted as a function of the 2MP loading. Here $Đ$ is the Maxwell-Stefan diffusivity, and r_c is the radius of the MFI crystals used in the experimental measurements. The thick solid lines are "guides to the eye".

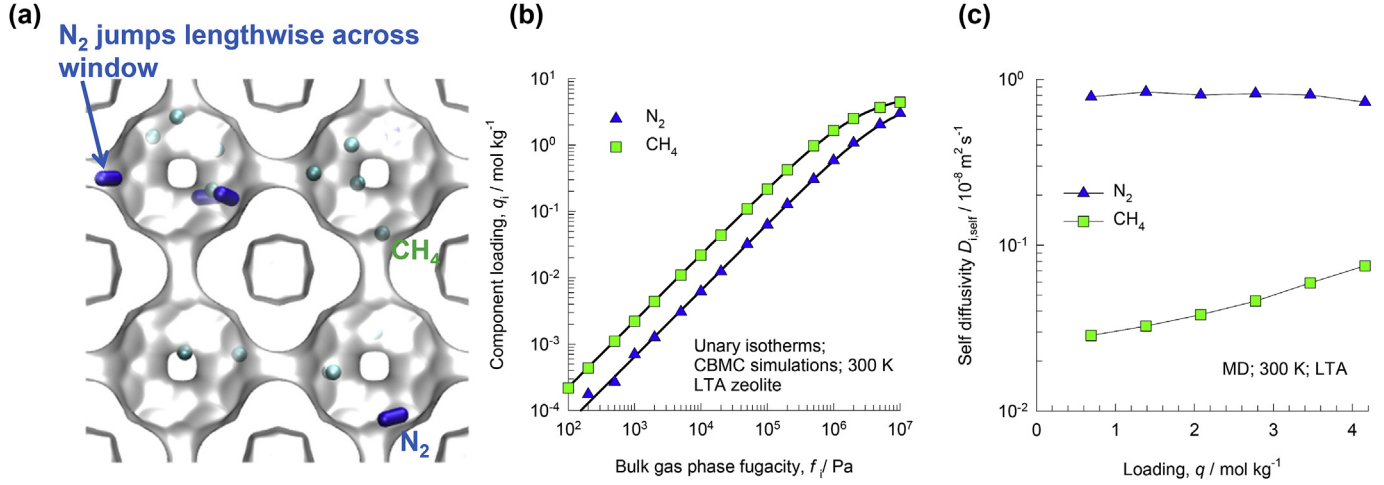

Fig. 18. (a) Snapshots showing the location of nitrogen and methane in LTA zeolite. (b) CBMC simulations of unary isotherms of N_2, and CH_4 in LTA at 300 K. (c) MD simulations of the unary diffusivities of N_2, and CH_4 in LTA at 300 K.

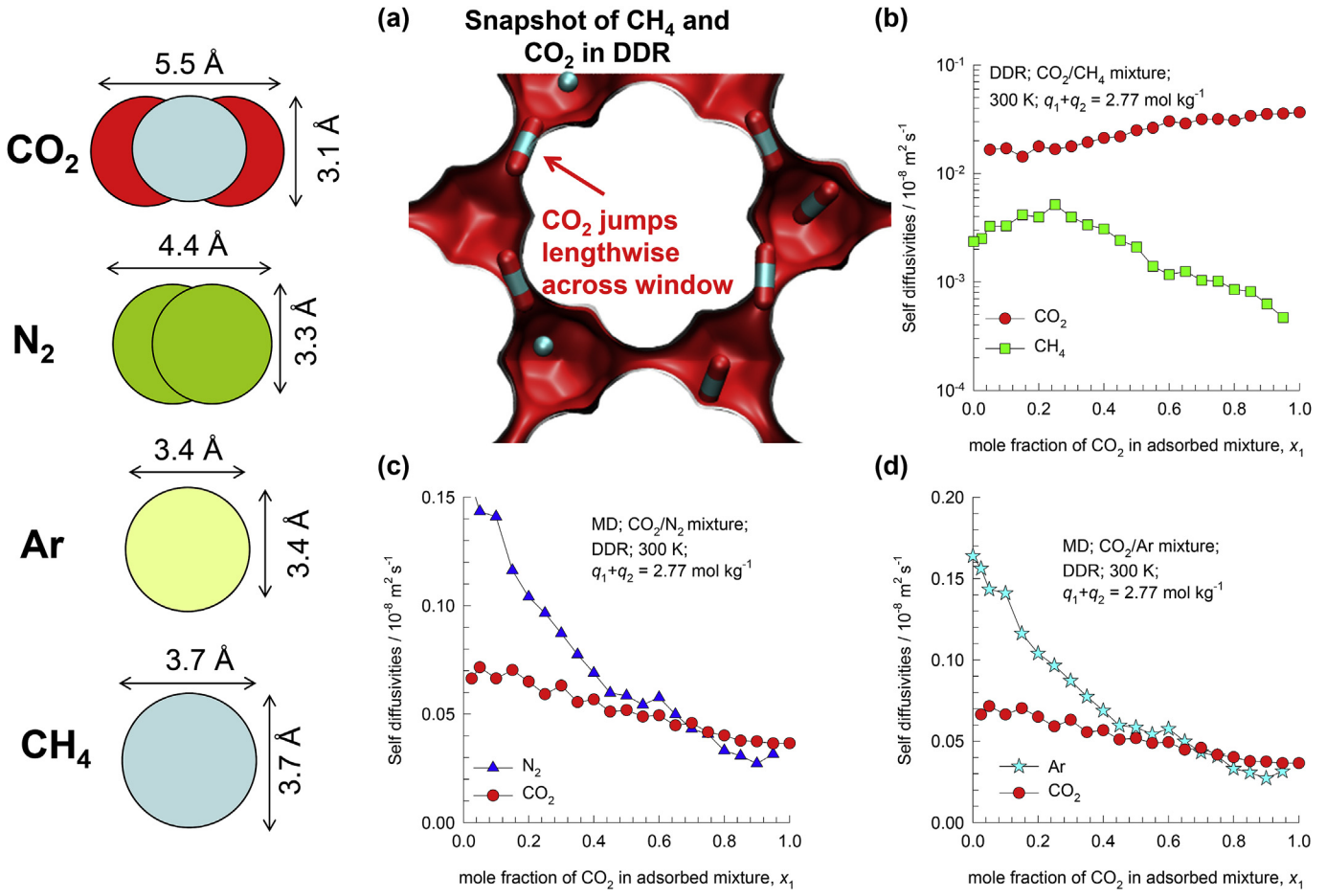

Fig. 19. (a) Snapshots showing the location of CO_2, and CH_4 for mixture adsorption in DDR at 300 K. (b, c, d) MD simulations of self-diffusivities (b) CO_2/CH_4, (c) CO_2/N_2 and (d) CO_2/Ar mixtures in DDR zeolite.

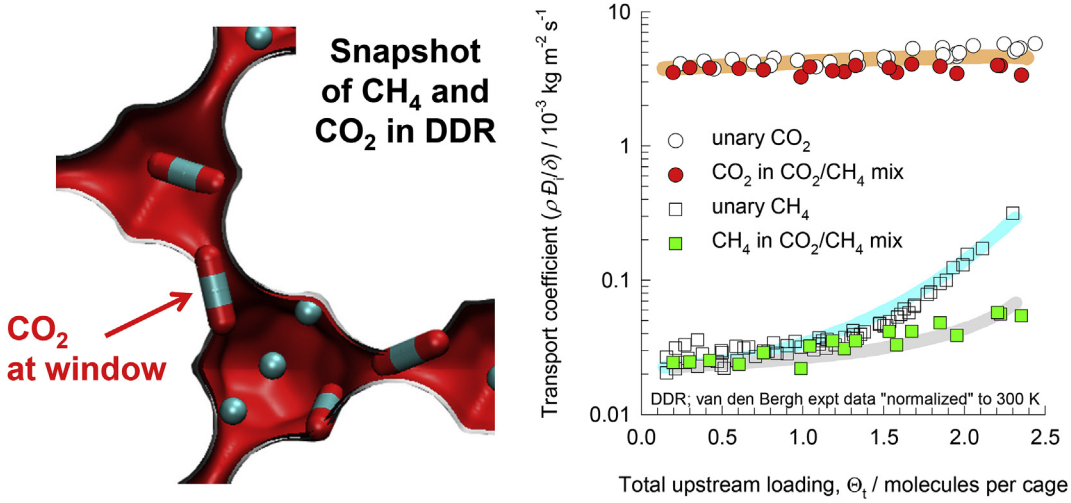

Fig. 20. Comparison of transport coefficients, $(\rho Đ_i/\delta)$, for CO_2 and CH_4, backed out from unary and binary mixture permeation data across DDR membrane [68,89,90], plotted against the total mixture loading at the upstream face of the membrane. Here ρ is the framework density, $Đ_i/\delta$ is the Maxwell-Stefan diffusivity, and δ is the thickness of the membrane layer. The thick solid lines are "guides to the eye".

data of Hasegawa et al. [100] show that the alcohol fluxes *decrease* with increasing water composition in the feed; see Fig. 24a–c. Indeed, *both* water and alcohol fluxes are reduced with increasing concentrations of partner species in the mixture The experimental data on pervaporation of water/ethanol mixtures across LTA-4A membrane [101], shown in Fig. 24d, can also be interpreted in terms of mutual-slowing down effects. Analogous experimental data for water/alcohol pervaporation across DDR membranes are also reported [102].

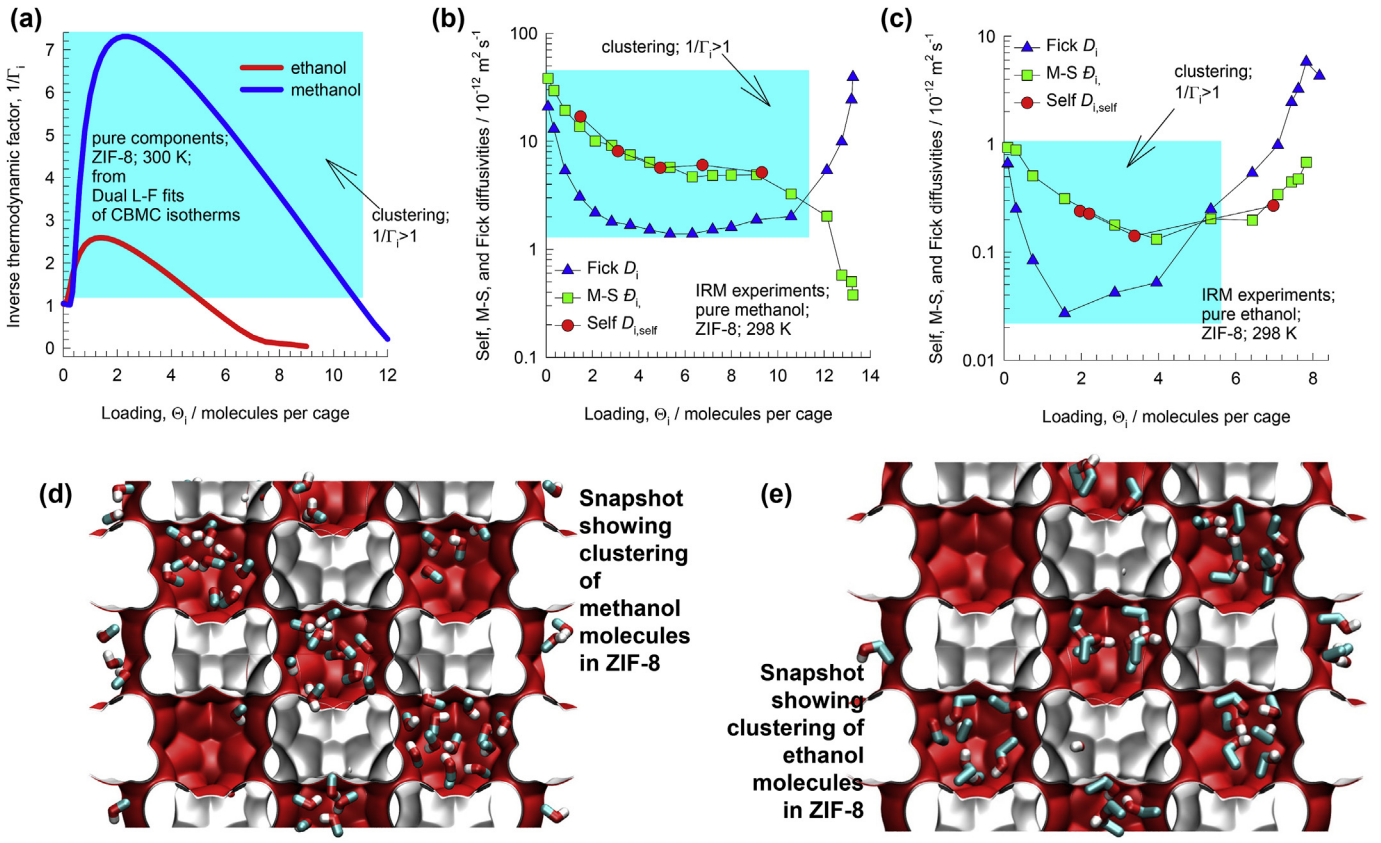

Fig. 21. (a) The inverse thermodynamic factor, $1/\Gamma$, for methanol and ethanol adsorption in ZIF-8, obtained from analytic differentiation of the dual-Langmuir-Freundlich fits. (b, c) Loading dependence of self-, Maxwell-Stefan, and Fick diffusivities of (a) methanol, and (b) ethanol in ZIF-8 [94]. (d, e) Snapshots showing the equilibrium positions of adsorbed (d) methanol, and (e) ethanol molecules in ZIF-8.

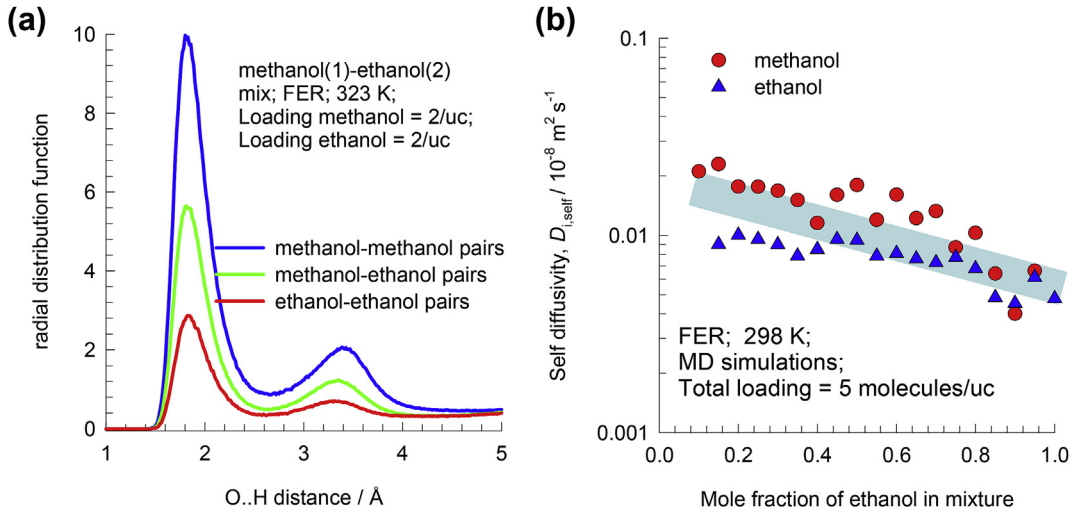

Fig. 22. (a) RDFs for binary methanol(1)/ethanol(2) mixtures at 323 K in FER with component loadings $\Theta_1 = \Theta_2 = 2$ uc^{-1}. (b) MD simulations for self-diffusivities in methanol/ethanol mixtures in FER zeolite at 298 K. The thick solid line is "guide to the eye".

7. Commensurate-incommensurate adsorption and diffusion

For separation of mixtures of aromatics, the principle of commensurate adsorption can be exploited by appropriate choice of the cross-sectional geometry of the channels [6]. These separations rely on matching the shape and size of the guest molecules with the shape and size of the channels. Torres-Knoop et al. [103,104] have provided examples in which optimum face-to-face stacking of aromatic molecules can lead to uncommonly effective separations. Within triangular channels of a structure such as $Fe_2(BDP)_3$, 1,3,5 tri-chlorobenzene (TCB) can be selectively separated from the 1,2,3 and 1,2,4 TCB isomers; see cartoon in Fig. 25a. The preferential adsorption of the 1,3,5 isomer is due to optimum face-to-face stacking.

Other cartoons of face-to-face stacking of aromatics are shown in Fig. 25b–f for commensurate adsorption of benzene, and p-

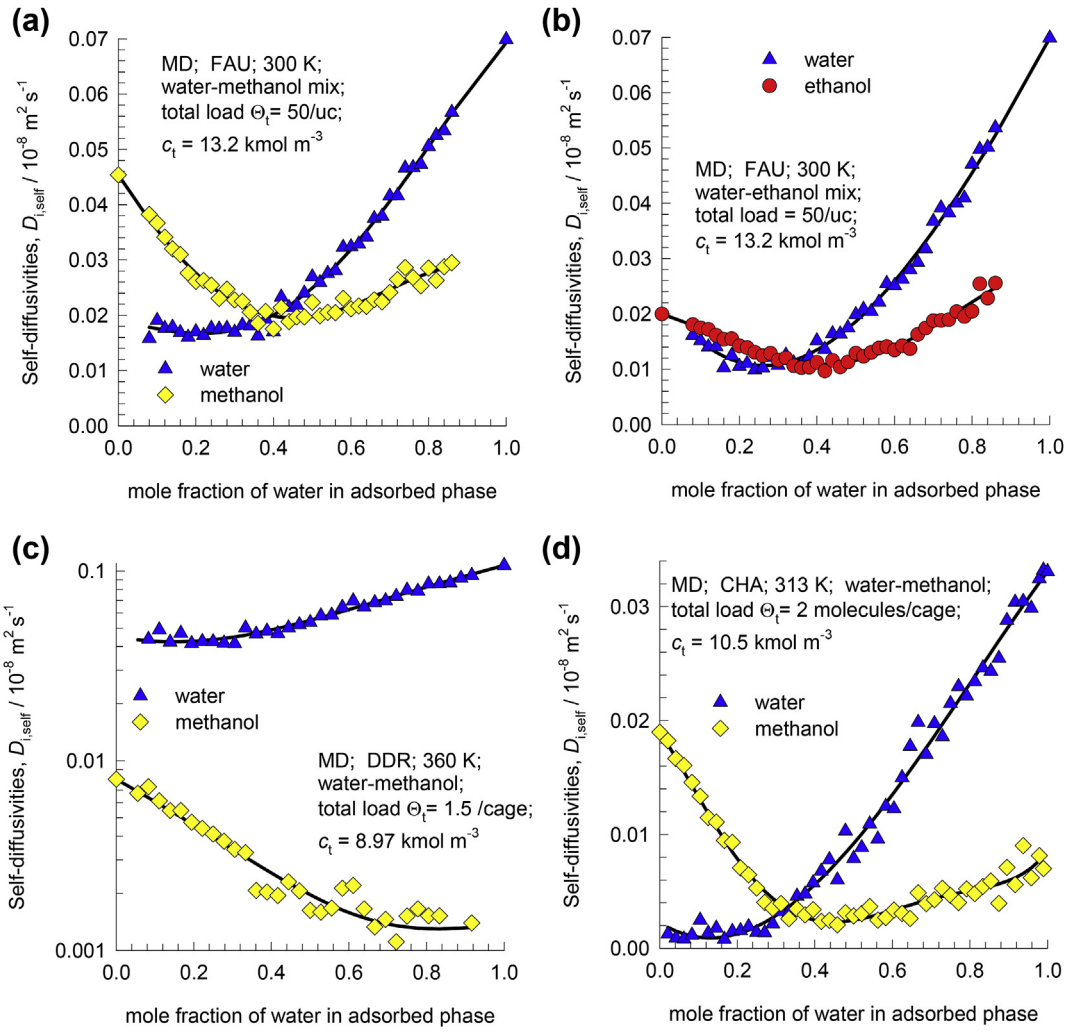

Fig. 23. Self-diffusivities in water/methanol, and water/ethanol mixtures of varying adsorbed phase compositions in (a, b) FAU, (c) DDR, and (d) CHA zeolites. The data are compiled from MD simulation results published in the literature [92,99,107].

xylene that are important feedstocks in the petrochemical industries. While commensurate adsorption is unusually effective for mixture separations [6], there are important consequences of diffusion, as explained below.

Let us consider the adsorption and diffusion of n-alkanes, with C numbers ranging from 1 to 7, in cobalt formate (Co-FA) framework [105]. The Co-FA structure consists of 1D zig-zag channels; one unit cell of Co-FA comprises a total of four distinct channel "segments"; each channel segment forms part of the repeat zig-zag structure; see Fig. 26a. The Henry coefficients for adsorption follows an unusual, non-monotonic, dependence on the C number: C1 < C2 < C3 > nC4 > nC5 < nC6 < nC7; see Fig. 26b. Confirmation of the unusual hierarchy in the adsorption strengths observed in Fig. 26b is provided by the experimental data of Li et al. [20] for unary isotherms of 1-propanol and 1-butanol in Co-Formate; the shorter alcohol is reported to have a higher adsorption strength than the longer chain alcohol. The hierarchy of self-diffusivities also shows non-monotonicity (cf. Fig. 26c); the hierarchy is the mirror image of that witnessed for Henry coefficients: C1 > C2 > C3 < nC4 < nC5 > nC6 > nC7. In order to understand unusual hierarchy of Henry coefficients and diffusivities, Fig. 27 presents computational snapshots of the conformations of adsorbed ethane (C2), propane (C3), and n-pentane (nC5) molecules within the zig-zag 1D channel segments of Co-Formate. The length of each channel segment is commensurate with that of the propane molecule and longer molecules such as n-pentane (nC5), and n-hexane (nC6) must straddle two channel segments. A simple physical reasoning is that commensurate adsorption implies that the molecules resides "cozily" within the channel segment, and has a low tendency to hop to a neighboring location. The converse is true for guests that adsorb incommensurately; that molecule feels "out of place" and has a tendency to escape and hop to a neighboring site. In order to get an appreciation of this unusual hierarchy and the influence of commensurate-incommensurate adsorption, see animations of the diffusion of methane (Video 33), ethane (Video 34), propane (Video 35), n-butane (Video 36), and n-pentane (Video 37) in the 1D channels of Co-FA.

Supplementary video related to this article can be found at http://dx.doi.org/10.1016/j.micromeso.2017.09.014.

8. *Cul-de-sacs* for molecular traffic

The molecular traffic in MOR zeolite (Mordenite, see Fig. 2), that consists of 12-ring (7.0 Å × 6.5 Å) 1D channels, connected to 8-ring (5.7 Å × 2.6 Å) side-pockets, exhibits unusual mixture diffusion effects. Computational snapshots (cf. Fig. 28a and b) of the location of molecules for CO_2/CH_4 and CO_2/N_2 mixture adsorption show that CO_2 gets preferentially ensconced in the side-pockets. The side

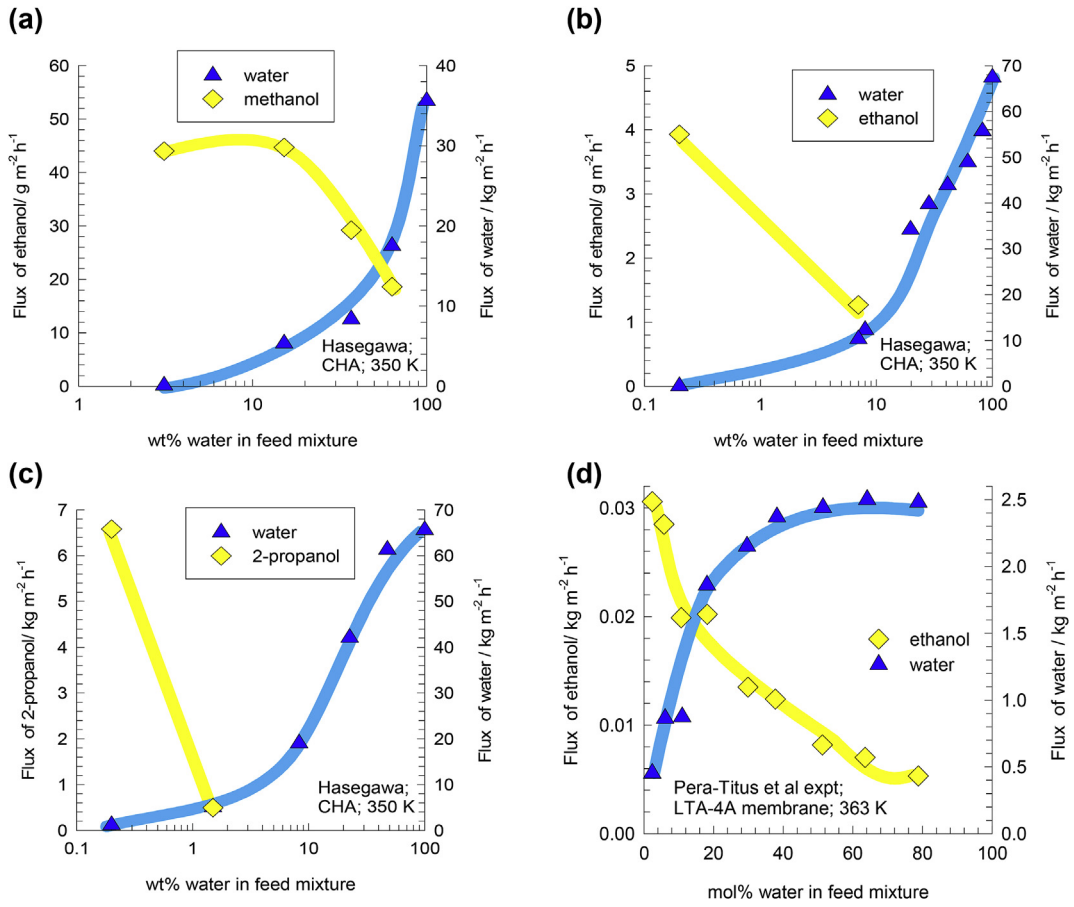

Fig. 24. (a, b, c) Experimental data of Hasegawa et al. [100] for permeation fluxes across CHA membrane as a function of the wt% water in (a) water/methanol, (b) water/ethanol, and (c) water/2-propanol mixtures. (d) Experimental data of Pera-Titus et al. [101] for the pervaporation fluxes of water and ethanol across LTA-4A membrane. The thick solid lines are "guides to the eye".

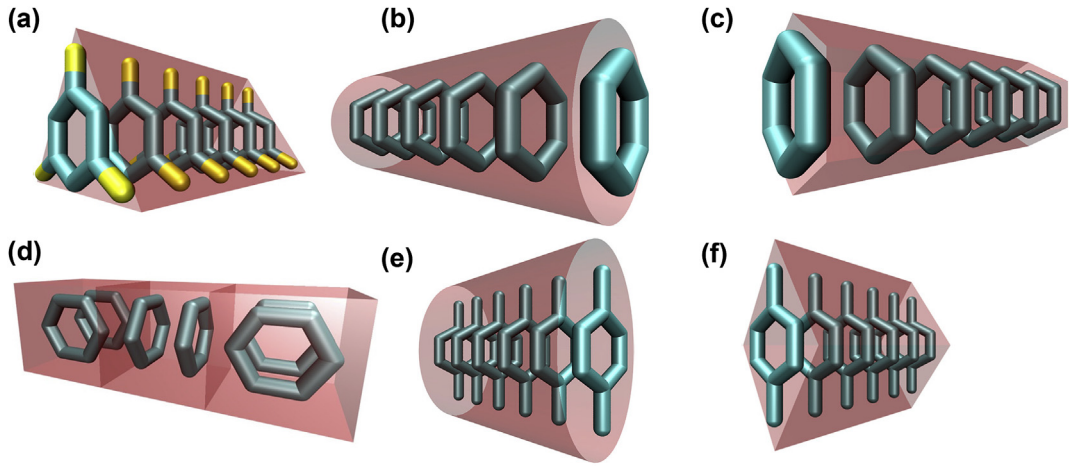

Fig. 25. Face-to-face stacking of molecules that have shapes that are commensurate with the channel cross-section. (a) triangular channels for triangular molecules (e.g. 1,3,5 trichlorbenzene, cyclo-propane, aluminum hydroxide). (a) cylindrical channels for molecules such as benzene, (c) honeycomb channels for hexagonal molecules (e.g. benzene), (d) cuboid channels for face-to-face stacking of benzene. (e) elliptical channels for face-to-face stacking of p-xylene, (f) diamond-like channels that allow face-to-face stacking of para-xylene.

pockets act like *cul-de-sacs* in respect of molecular traffic for CO_2. The near-stagnancy of CO_2 molecules located in the side pockets can be discerned by viewing Video 38, and Video 39. These animations of the molecular traffic demonstrate that CO_2 molecules located in side pockets appear to be "locked in" and do not participate in the main thoroughfare along the 12-ring channels [106]. An important consequence of the *cul-de-sac* effect is that the diffusivity of CO_2 in CO_2/CH_4 mixtures is about an order of magnitude lower than that of CH_4 when compared at mixture loadings below about 1.5 mol kg^{-1}; see Fig. 28c.

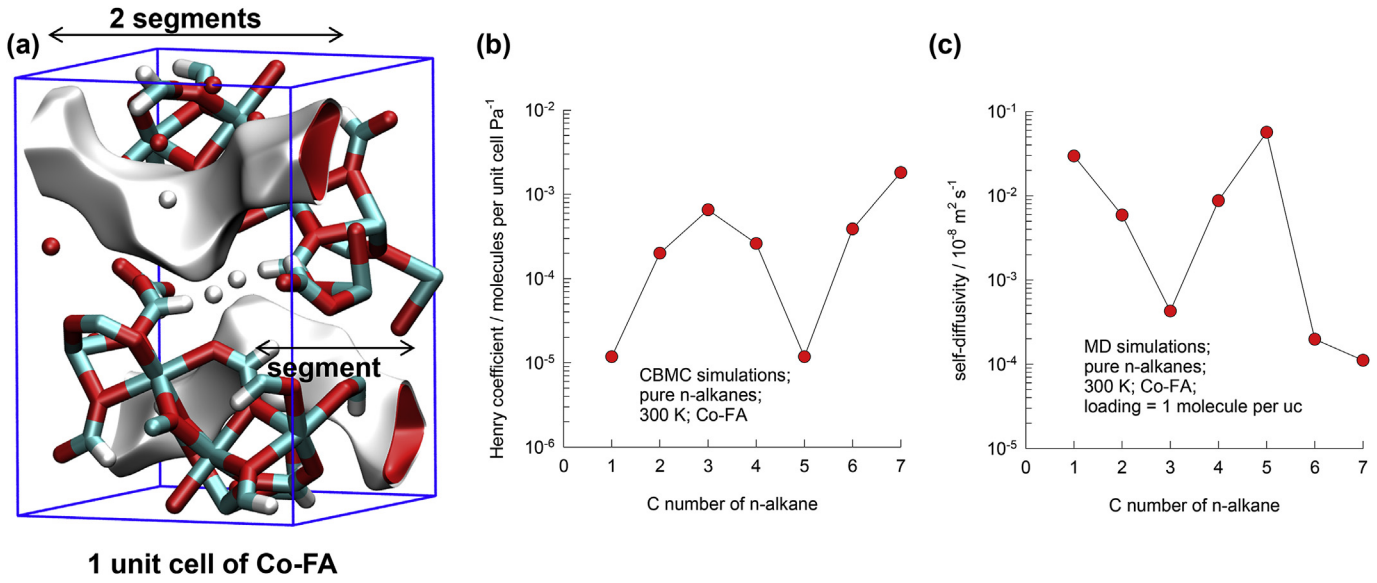

Fig. 26. (a) Pore landscape of one unit cell of Co-Formate. (b) Henry coefficients for adsorption of n-alkanes in Co-Formate as a function of C number. (c) Self-diffusivity for n-alkanes in Co-Formate as a function of C number.

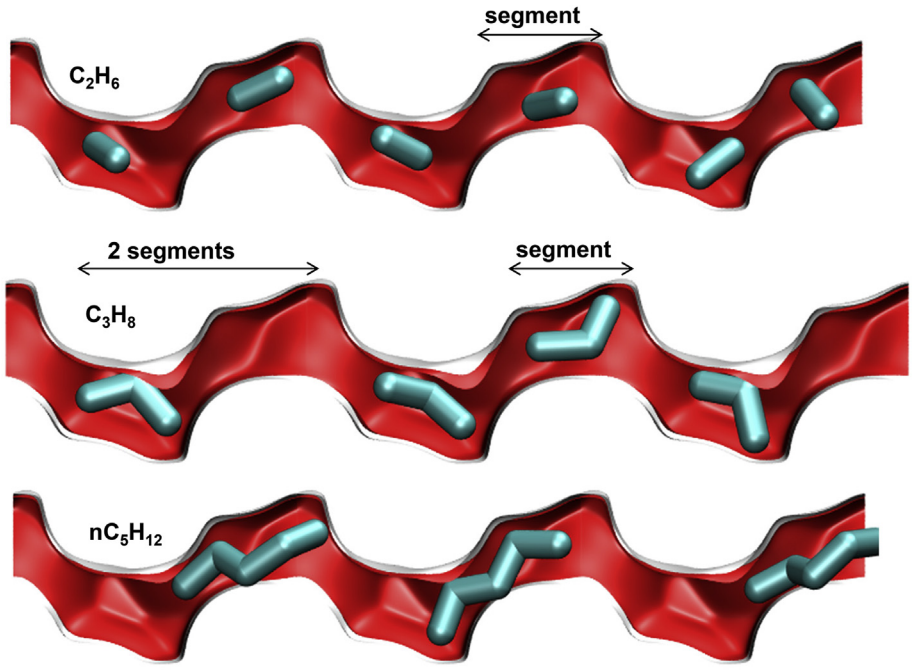

Fig. 27. Snapshots showing the location and conformations of ethane, propane, and n-pentane molecules within the zig-zag 1D channel segments of Co-Formate.

Supplementary video related to this article can be found at http://dx.doi.org/10.1016/j.micromeso.2017.09.014.

9. Conclusions

Using MD simulations, along with computational snapshots and video animations, a number of experimental observations of mixture diffusion in microporous crystalline materials can be rationalized and explained. The important messages emerging from this article are summarized below.

- Slowing-down effects are often significant for mixture diffusion in microporous materials. Broadly speaking, the motion of the more-mobile-less-strongly adsorbed component is retarded by the tardier-more-strongly-adsorbed component.
- Traffic junction effects in MFI zeolite of importance of diffusion of mixtures of (a) linear and branched alkanes, (b) alkanes/aromatics, and (c) alkenes/aromatics.
- In cage-type materials such as DDR, LTA, CHA, and ZIF-8, molecules jump on-at-a-time across the narrow windows; the inter-cage jumps are uncorrelated. Pencil-like molecules such as CO_2, and N_2 hop length-wise across the windows.

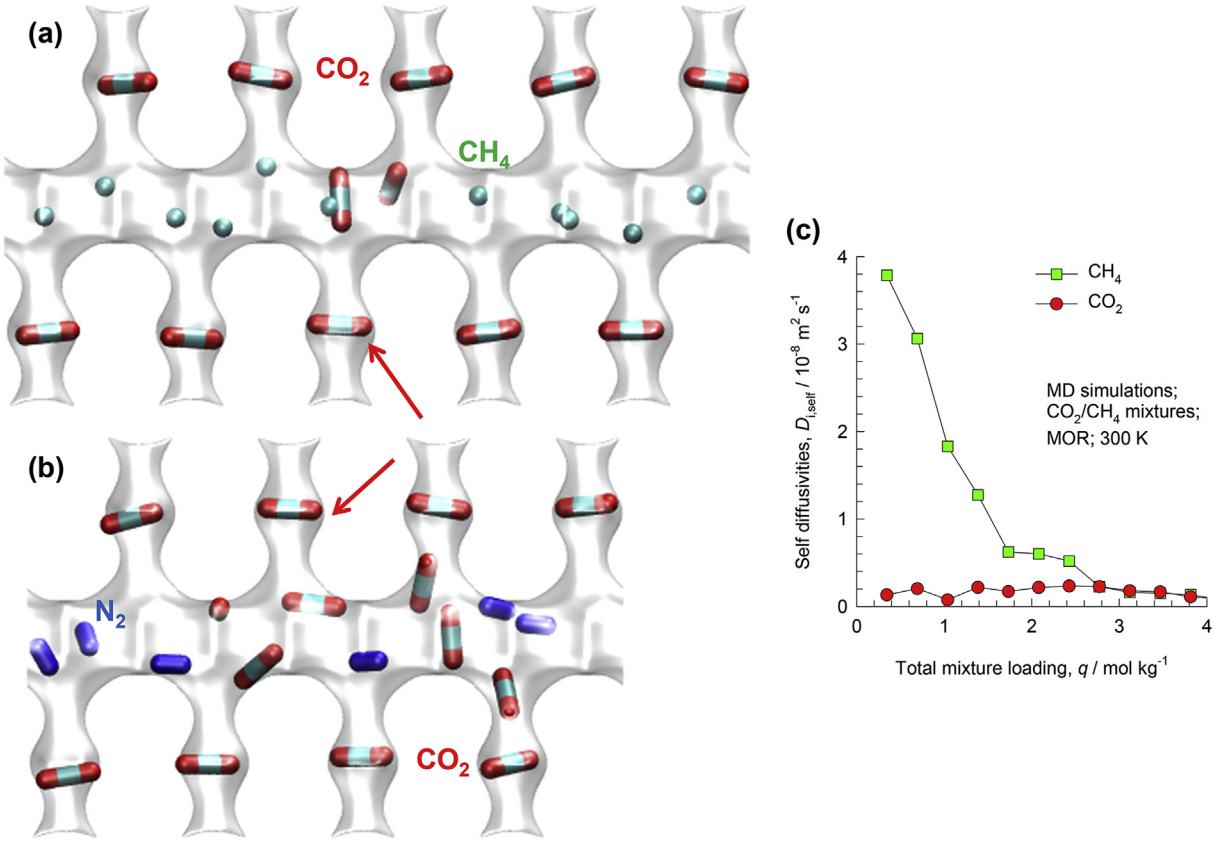

Fig. 28. (a, b) Snapshots of (a) CO_2/CH_4 and (b) CO_2/N_2 mixture adsorption in MOR. (b) MD simulations of the self-diffusivities of CO_2, and CH_4 as a function of the total mixture loading, $q_1 + q_2$, keeping $q_1 = q_2$.

- For CO_2 capture from CO_2/CH_4, CO_2/N_2, and CO_2/Ar mixtures, the preferential location of CO_2 in the window regions of DDR and ZIF-8 causes the suppression of the inter-cage hopping of partner molecules, resulting in increasing selectivities in favor of CO_2.
- Due to hydrogen bonding between water and alcohol, mutual-slowing down effects are important for water/alcohols mixture diffusion.
- Commensurate adsorption of a guest species often implies that its mobility within the framework will be restricted. A guest species that adsorbs incommensurately, has a higher tendency to jump to a neighboring site.
- The preferential location of CO_2 within the side-pockets of MOR zeolite, results in a significantly lowered diffusivity due to the *cul-de-sac* nature of the side pockets.

Though the discussions in this article are largely qualitative in nature, the obtained insights should aid in setting up rigorous quantitative models for mixture diffusion using the Maxwell-Stefan (M-S) diffusion formulation [16,66,67]. Using judicious inputs from MD simulation data, the M-S diffusion formulation has been particularly successful in the modeling of slowing-down effects [66,75], traffic junction effects [59,84], and transient overshoots [5,55]. However, the phenomena of mutual-slowing down due to molecular clustering, as highlighted in this paper, cannot be modeled using the current version of the M-S formulation; the exchange coefficients $Đ_{ij}$ in the M-S formulation only cater for slowing down of the more mobile partners [67,92,107]. The M-S formulation, in its current form, also fails to properly account for hindering effects due to preferential location of CO_2 at windows, pockets, and cul-de-sacs [108]. There is an urgent need to extend the M-S formulation to take account of molecular clustering, and hindering effects.

Notation

$D_{i,eff}$	effective Fick diffusivity, $m^2\ s^{-1}$
$Đ_i$	Maxwell-Stefan diffusivity, $m^2\ s^{-1}$
f	fugacity of species, Pa
f_t	total fugacity of bulk fluid mixture, Pa
N_i	molar flux of species i, mol $m^{-2}\ s^{-1}$
p_i	partial pressure of species i in mixture, Pa
p_t	total system pressure, Pa
q_i	component molar loading of species i, mol kg^{-1}
q_t	total molar loading for mixture adsorption, mol kg^{-1}
r_c	radius of crystallite, m
T	absolute temperature, K
z	distance along membrane layher, m

Greek letters

δ	thickness of membrane layer, m
Γ	thermodynamic correction factor, dimensionless
Π_i	membrane permeance of species i, mol $m^{-2}\ s^{-1}\ Pa^{-1}$
Θ	loading of species, molecules per unit cage, or per unit cell
Θ_t	total mixture loading, molecules per unit cage, or per unit cell
ρ	framework density, kg m^{-3}

Subscripts

i	referring to component i

0	upstream face of membrane
1	referring to species 1
2	referring to species 2
i,j	components in mixture
t	referring to total mixture
δ	downstream face of membrane

References

[1] D.M. Ruthven, Principles of Adsorption and Adsorption Processes, John Wiley, New York, 1984.
[2] J. Kärger, D.M. Ruthven, D.N. Theodorou, Diffusion in Nanoporous Materials, Wiley - VCH, Weinheim, 2012.
[3] R. Krishna, RSC Adv. 5 (2015) 52269–52295.
[4] R. Krishna, RSC Adv. 7 (2017) 35724–35737.
[5] R. Krishna, R. Baur, J.M. Van Baten, React. Chem. Eng. 2 (2017) 324–336.
[6] R. Krishna, J.M. van Baten, Phys. Chem. Chem. Phys. 19 (2017) 20320–20337.
[7] Z. Bao, G. Chang, H. Xing, R. Krishna, Q. Ren, B. Chen, Energy Environ. Sci. 9 (2016) 3612–3641.
[8] K. Sumida, D.L. Rogow, J.A. Mason, T.M. McDonald, E.D. Bloch, Z.R. Herm, T.-H. Bae, J.R. Long, Chem. Rev. 112 (2012) 724–781.
[9] Y. He, R. Krishna, B. Chen, Energy Environ. Sci. 5 (2012) 9107–9120.
[10] Y.J. Colón, R.Q. Snurr, Chem. Soc. Rev. 43 (2014) 5735–5749.
[11] J. Caro, Curr. Opin. Chem. Eng. 1 (2011) 77–83.
[12] L. Sandström, E. Sjöberg, J. Hedlund, J. Membr. Sci. 380 (2011) 232–240.
[13] P. Kortunov, L. Heinke, M. Arnold, Y. Nedellec, D.J. Jones, J. Caro, J. Kärger, J. Am. Chem. Soc. 129 (2007) 8041–8047.
[14] Y.S. Li, F.Y. Liang, H. Bux, A. Veldhoff, W.S. Yang, J. Caro, Angew. Chem. Int. Ed. 49 (2010) 548–551.
[15] A. Huang, H. Bux, F. Steinbach, J. Caro, Angew. Chem. Int. Ed. 122 (2010) 5078–5081.
[16] R. Krishna, Microporous Mesoporous Mater. 185 (2014) 30–50.
[17] D.M. Ruthven, S. Farooq, K.S. Knaebel, Pressure Swing Adsorption, VCH Publishers, New York, 1994.
[18] G.F. Froment, K.B. Bischoff, Chemical Reactor - Analysis and Design, John Wiley & Sons, New York, 1979.
[19] R. Baur, R. Krishna, Catal. Today 105 (2005) 173–179.
[20] K. Li, D.H. Olson, J.Y. Lee, W. Bi, K. Wu, T. Yuen, Q. Xu, J. Li, Adv. Funct. Mater. 18 (2008) 2205–2214.
[21] V. Finsy, H. Verelst, L. Alaerts, D. De Vos, P.A. Jacobs, G.V. Baron, J.F.M. Denayer, J. Am. Chem. Soc. 130 (2008) 7110–7118.
[22] D.S. Coombes, F. Corà, C. Mellot-Draznieks, R.G. Bell, J. Phys. Chem. C 113 (2009) 544–552.
[23] C. Serre, F. Millange, C. Thouvenot, M. Nouguès, G. Marsolier, D. Louër, G. Férey, J. Am. Chem. Soc. 124 (2002) 13519–13526.
[24] H.J. Choi, M. Dincă, J.R. Long, J. Am. Chem. Soc. 130 (2008) 7848–7850.
[25] P.S. Bárcia, F. Zapata, J.A.C. Silva, A.E. Rodrigues, B. Chen, J. Phys. Chem. B 111 (2008) 6101–6103.
[26] H. Wang, J. Getzschmann, I. Senkovska, S. Kaskel, Microporous Mesoporous Mater. 116 (2008) 653–657.
[27] D. Dubbeldam, K.S. Walton, D.E. Ellis, R.Q. Snurr, Angew. Chem. Int. Ed. 46 (2007) 4496–4499.
[28] C. Chmelik, J. Kärger, M. Wiebcke, J. Caro, J.M. van Baten, R. Krishna, Microporous Mesoporous Mater. 117 (2009) 22–32.
[29] C. Baerlocher, L.B. McCusker, Database of Zeolite Structures, International Zeolite Association, 12 October 2004. http://www.iza-structure.org/databases/.
[30] R. Krishna, Chem. Soc. Rev. 41 (2012) 3099–3118.
[31] R. Krishna, J. Phys. Chem. C 113 (2009) 19756–19781.
[32] R. Krishna, J.M. van Baten, J. Phys. Chem. C 116 (2012) 23556–23568.
[33] R. Krishna, J.M. van Baten, J. Membr. Sci. 430 (2013) 113–128.
[34] R. Krishna, J.M. van Baten, Phys. Chem. Chem. Phys. 15 (2013) 7994–8016.
[35] R. Krishna, J.M. van Baten, Microporous Mesoporous Mater. 109 (2008) 91–108.
[36] R. Krishna, J.M. van Baten, Microporous Mesoporous Mater. 107 (2008) 296–298.
[37] R. Krishna, J.M. van Baten, J. Phys. Chem. C 114 (2010) 18017–18021.
[38] R. Krishna, J.M. van Baten, Microporous Mesoporous Mater. 137 (2011) 83–91.
[39] A.F. Combariza, G. Sastre, A. Corma, J. Phys. Chem. C 113 (2009) 11246–11253.
[40] P. Demontis, G.B. Suffritti, Microporous Mesoporous Mater. 125 (2009) 160–168.
[41] S. Fritzsche, M. Wolfsberg, R. Haberlandt, P. Demontis, G.B. Suffritti, A. Tilocca, Chem. Phys. Lett. 296 (1998) 253–258.
[42] A. García-Sánchez, D. Dubbeldam, S. Calero, J. Phys. Chem. C 114 (2010) 15068–15074.
[43] F. Salles, A. Ghoufi, G. Maurin, R.G. Bell, C. Mellot-Draznieks, G. Férey, Angew. Chem. Int. Ed. 47 (2008) 8487–8491.
[44] D. Dubbeldam, R. Krishna, R.Q. Snurr, J. Phys. Chem. C 113 (2009) 19317–19327.
[45] D. Dubbeldam, G.A.E. Oxford, R. Krishna, L.J. Broadbelt, R.Q. Snurr, J. Chem. Phys. 133 (2010) 034114.
[46] D.C. Ford, D. Dubbeldam, R.Q. Snurr, Diffus. Fundam. 11 (2009) 78.
[47] K. Seehamart, T. Nanok, R. Krishna, J.M. van Baten, T. Remsungnen, S. Fritzsche, Microporous Mesoporous Mater. 125 (2009) 97–100.
[48] D. Peralta, G. Chaplais, A. Simon-Masseron, K. Barthelet, C. Chizallet, A.-A. Quoineaud, G.D. Pirngruber, J. Am. Chem. Soc. 134 (2012) 8115–8126.
[49] D. Peralta, G. Chaplais, A. Simon-Masseron, K. Barthelet, G.D. Pirngruber, Ind. Eng. Chem. Res. 51 (2012) 4692–4702.
[50] L. Li, R. Krishna, Y. Wang, X. Wang, J. Yang, J. Li, Eur. J. Inorg. Chem. 2016 (2016) 4457–4462, http://dx.doi.org/10.1002/ejic.201600182.
[51] L. Li, R. Krishna, Y. Wang, J. Yang, X. Wang, J. Li, J. Mater. Chem. A 4 (2016) 751–755.
[52] H.W. Habgood, Canad. J. Chem. 36 (1958) 1384–1397.
[53] S.J. Bhadra, S. Farooq, Ind. Eng. Chem. Res. 50 (2011) 14030–14045.
[54] B. Majumdar, S.J. Bhadra, R.P. Marathe, S. Farooq, Ind. Eng. Chem. Res. 50 (2011) 3021–3034.
[55] R. Krishna, Phys. Chem. Chem. Phys. 18 (2016) 15482–15495.
[56] R. Krishna, J.M. van Baten, J. Membr. Sci. 360 (2010) 323–333.
[57] J. Caro, M. Noack, Microporous Mesoporous Mat. 115 (2008) 215–233.
[58] C. Baerlocher, W.M. Meier, D.H. Olson, Atlas of Zeolite Framework Types, Elsevier, Amsterdam, 2002.
[59] N. Hansen, R. Krishna, J.M. van Baten, A.T. Bell, F.J. Keil, J. Phys. Chem. C 113 (2009) 235–246.
[60] N. Hansen, R. Krishna, J.M. van Baten, A.T. Bell, F.J. Keil, Chem. Eng. Sci. 65 (2010) 2472–2480.
[61] C. Förste, A. Germanus, J. Kärger, H. Pfeifer, J. Caro, W. Pilz, A. Zikánová, J. Chem. Soc. Faraday Trans. 1 (83) (1987) 2301–2309.
[62] M. Fernandez, J. Kärger, D. Freude, A. Pampel, J.M. van Baten, R. Krishna, Microporous Mesoporous Mater. 105 (2007) 124–131.
[63] H. Bux, C. Chmelik, R. Krishna, J. Caro, J. Membr. Sci. 369 (2011) 284–289.
[64] H. Bux, C. Chmelik, J.M. Van Baten, R. Krishna, J. Caro, Adv. Mater. 22 (2010) 4741–4743.
[65] R. Krishna, J.M. van Baten, Phys. Chem. Chem. Phys. 13 (2011) 10593–10616.
[66] R. Krishna, J.M. van Baten, J. Membr. Sci. 383 (2011) 289–300.
[67] R. Krishna, J. Membr. Sci. 540 (2017) 261–276.
[68] C. Chmelik, J.M. van Baten, R. Krishna, J. Membr. Sci. 397–398 (2012) 87–91.
[69] D. Dubbeldam, R.Q. Snurr, Mol. Simul. 33 (2007) 15–30.
[70] B. Smit, T.L.M. Maesen, Chem. Rev. 108 (2008) 4125–4184.
[71] F.J. Keil, R. Krishna, M.O. Coppens, Rev. Chem. Eng. 16 (2000) 71–197.
[72] J. Jiang, R. Babarao, Z. Hu, Chem. Soc. Rev. 40 (2011) 3599–3612.
[73] D. Frenkel, B. Smit, Understanding Molecular Simulations: from Algorithms to Applications, Academic Press, San Diego, 2002.
[74] T.J.H. Vlugt, J.P.J.M. Van der Eerden, M. Dijkstra, B. Smit, D. Frenkel, Introduction to molecular simulation and statistical thermodynamics Universiteit Utrecht. http://www.phys.uu.nl/~vlugt/imsst/, 1 January 2008.
[75] R. Krishna, J.M. van Baten, J. Membr. Sci. 377 (2011) 249–260.
[76] E.D. Bloch, W.L. Queen, R. Krishna, J.M. Zadrozny, C.M. Brown, J.R. Long, Science 335 (2012) 1606–1610.
[77] J.M. van de Graaf, F. Kapteijn, J.A. Moulijn, A. I. Ch. E. J. 45 (1999) 497–511.
[78] T.J.H. Vlugt, W. Zhu, F. Kapteijn, J.A. Moulijn, B. Smit, R. Krishna, J. Am. Chem. Soc. 120 (1998) 5599–5600.
[79] T.J.H. Vlugt, R. Krishna, B. Smit, J. Phys. Chem. B 103 (1999) 1102–1118.
[80] R. Krishna, B. Smit, S. Calero, Chem. Soc. Rev. 31 (2002) 185–194.
[81] M. Schenk, S.L. Vidal, T.J.H. Vlugt, B. Smit, R. Krishna, Langmuir 17 (2001) 1558–1570.
[82] C. Chmelik, L. Heinke, J.M. van Baten, R. Krishna, Microporous Mesoporous Mater. 125 (2009) 11–16.
[83] D. Schuring, A.P.J. Jansen, R.A. van Santen, J. Phys. Chem. B 104 (2000) 941–948.
[84] T. Titze, C. Chmelik, J. Kärger, J.M. van Baten, R. Krishna, J. Phys. Chem. C 118 (2014) 2660–2665.
[85] R. Krishna, J.M. van Baten, Chem. Eng. Sci. 64 (2009) 3159–3178.
[86] T. Binder, A. Lauerer, C. Chmelik, J. Haase, J. Kärger, D.M. Ruthven, Ind. Eng. Chem. Res. 54 (2015) 8997–9004.
[87] A. Lauerer, T. Binder, C. Chmelik, E. Miersemann, J. Haase, D.M. Ruthven, J. Kärger, Nat. Commun. 6 (2015) 7697, http://dx.doi.org/10.1038/ncomms8697.
[88] R. Krishna, J.M. van Baten, Sep. Purif. Technol. 61 (2008) 414–423.
[89] J. van den Bergh, W. Zhu, J. Gascon, J.A. Moulijn, F. Kapteijn, J. Membr. Sci. 316 (2008) 35–45.
[90] J. van den Bergh, W. Zhu, J.C. Groen, F. Kapteijn, J.A. Moulijn, K. Yajima, K. Nakayama, T. Tomita, S. Yoshida, Stud. Surf. Sci. Catal. 170 (2007) 1021–1027.
[91] R. Krishna, J.M. van Baten, Sep. Purif. Technol. 76 (2011) 325–330.
[92] R. Krishna, J.M. van Baten, Langmuir 26 (2010) 10854–10867.
[93] J.Y. Wu, Q.L. Liu, Y. Xiong, A.M. Zhu, Y. Chen, J. Phys. Chem. B 113 (2009) 4267–4274.
[94] C. Chmelik, H. Bux, J. Caro, L. Heinke, F. Hibbe, T. Titze, J. Kärger, Phys. Rev. Lett. 104 (2010) 085902.
[95] C. Zhang, X. Yang, Fluid Phase Equilib. 231 (2005) 1–10.
[96] J. Kärger, T. Binder, C. Chmelik, F. Hibbe, H. Krautscheid, R. Krishna, J. Weitkamp, Nat. Mater. 13 (2014) 333–343.
[97] R. Krishna, J.M. van Baten, Langmuir 26 (2010) 3981–3992.
[98] R. Krishna, J.M. van Baten, Langmuir 26 (2010) 8450–8463.

[99] R. Krishna, J.M. van Baten, J. Phys. Chem. C 114 (2010) 13154–13156.
[100] Y. Hasegawa, C. Abe, M. Nishioka, K. Sato, T. Nagase, T. Hanaoka, J. Membr. Sci. 364 (2010) 318–324.
[101] M. Pera-Titus, C. Fité, V. Sebastián, E. Lorente, J. Llorens, F. Cunill, Ind. Eng. Chem. Res. 47 (2008) 3213–3224.
[102] J. Kuhn, J.M. Castillo-Sanchez, J. Gascon, S. Calero, D. Dubbeldam, T.J.H. Vlugt, F. Kapteijn, J. Gross, J. Phys. Chem. C 113 (2009) 14290–14301.
[103] A. Torres-Knoop, S.R.G. Balestra, R. Krishna, S. Calero, D. Dubbeldam, ChemPhysChem 16 (2015) 532–535.
[104] A. Torres-Knoop, D. Dubbeldam, ChemPhysChem 16 (2015) 2046–2067.
[105] R. Krishna, J.M. van Baten, Mol. Simul. 35 (2009) 1098–1104.
[106] R. Krishna, J.M. van Baten, Chem. Eng. Sci. 63 (2008) 3120–3140.
[107] R. Krishna, J.M. van Baten, J. Membr. Sci. 360 (2010) 476–482.
[108] R. Krishna, J.M. van Baten, Sep. Purif. Technol. 60 (2008) 315–320.
[109] D. Keffer, V. Gupta, D. Kim, E. Lenz, H.T. Davis, A.V. McCormick, J. Mol. Graph. 14 (1996) 108–116.
[110] K. Sato, K. Sugimoto, N. Shimosuma, T. Kikuchi, T. Kyotani, T. Kurata, J. Membr. Sci. 409–410 (2012) 82–95.
[111] R. Krishna, J.M. van Baten, Chem. Eng. J. 140 (2008) 614–620.